AIBP-CAV1-VEGFR3 axis dictates lymphatic cell fate and controls lymphangiogenesis

Xiaojie Yang
Jun-dae Kim
Houston Methodist Research Institute
Kelvin Chan
Boston Children's Hospital
Qilin Gu
Jonathan Astin
The University of Auckland https://orcid.org/0000-0002-3554-0133
Philip Crosier
The University of Auckland
Pengchun Yu
Oklahoma Medical Research Foundation
Stanley Rockson
School of Medicine, Stanford University
Hong 2 Chen
Boston Children's Hospital
Longhou Fang (lhfang@houstonmethodist.org)
Houston Methodist Research Institute https://orcid.org/0000-0003-1653-5221

Article

Keywords: lymphatics, cholesterol, APOA1, AIBP, CAV-1

Posted Date: September 24th, 2021

DOI: https://doi.org/10.21203/rs.3.rs-905140/v1

AIBP-CAV1-VEGFR3 axis dictates lymphatic cell fate and controls lymphangiogenesis

Xiaojie Yang[1,9], Jun-dae Kim[1,9*], Siu-Lung Chan[2], Qilin Gu[1], Jonathan Astin[3], Philip S Crosier[3], Pengchun Yu[4], Stanley G Rockson[5], Hong Chen[2,*], and Longhou Fang[1,6,7,8,*]

[1]Center for Cardiovascular Regeneration, Department of Cardiovascular Sciences, Houston Methodist Research Institute. Houston Methodist, 6550 Fannin Street, Texas 77030, USA.

[2]Vascular Biology Program, Boston Children's Hospital, Harvard Medical School, Boston, MA 02115, USA

[3]Department of Molecular Medicine & Pathology, School of Medical Sciences, University of Auckland, Auckland 92019, New Zealand.

[4]Cardiovascular Biology Research Program, Oklahoma Medical Research Foundation 825 N.E. 13th Street Oklahoma City, OK 73104.

[5]Center for Lymphatic and Venous Disorders, Stanford University School of Medicine, 300 Pasteur Drive, Stanford, CA 94305.

[6]Department of Ophthalmology-Blanton Eye Institute,

[7]Houston Methodist Institute for Academic Medicine, Houston Methodist Research Institute. Houston Methodist, 6550 Fannin Street, Texas 77030, USA.

[8]Department of Cardiothoracic Surgeries, Weill Cornell Medical College, Cornell University, New York 10065, USA.

[9]Contributed equally

*correspondence: Jkim3@houstonmethodist.org, hong.chen@childrens.harvard.edu, or lhfang@houstonmethodist.org.

Abstract

The lymphatics control tissue fluid homeostasis; its dysfunction contributes to lymphedema. VEGFR3 signaling dictates LEC fate specification and lymphangiogenesis. Cholesterol is essential for cell function and organ development, yet the molecular mechanism by which cholesterol controls lymphangiogenesis is unknown. Here, we show that APOA1 binding protein (AIBP), a secreted protein, enhances LEC specification and increases lymphangiogenesis. Mechanistically, AIBP-mediated cholesterol efflux disrupts LEC caveolae, which abolishes CAV-1-dependent inhibition of VEGFR3 signaling. Loss of Aibp2, the zebrafish paralog of human AIBP, reduces LEC progenitors and impairs lymphangiogenesis; the impairment can be rescued by caveolae disruption. CAV-1 mutant that is deficient in VEGFR3 binding, thereby abolishing its inhibition, enhances VEGFR3 signaling and accelerates lymphatic growth. Furthermore, AIBP expression is reduced in the epidermis of human lymphedema. Administrating recombinant AIBP augments VEGFC-induced lymphangiogenesis and increases secondary tail lymphedema resolution in adult mice. Our studies reveal AIBP and CAV-1 as critical regulators of VEGFR3 signaling and identify previously unidentified therapeutic targets for lymphedema treatment.

Introduction

Lymphatic vasculature is essential for maintaining interstitial fluid homeostasis, dietary lipid transport and immune surveillance [1-4]. A lymphatic contribution is implicated in the pathogenesis of a variety of diseases, including lymphedema, tumor metastasis, cardiovascular disease, obesity, and diabetic mellitus [5-12]. Therapeutic augmentation of lymphangiogenesis has been documented to improve lymphatic structure and function [1-3, 8, 9]. Earlier studies show that the lymphatic system is derived from the embryonic cardinal vein (CV), where lymphatic endothelial cells (LEC) progenitors are specified and subsequently migrate and establish the lymphatic network [1-3, 13, 14]. Recent studies indicate that a subset of lymphatics can be developed through non-canonical mechanisms [15-20]. During murine development, the assembly of the lymphatic vascular network is initiated at approximately embryonic day 9.5 (E9.5) [21] under the control of VEGFC signaling through its cognate receptor VEGFR3 [22, 23]. LEC fate commitment occurs through SOX18-induced expression of PROX-1, which, in concert with the orphan nuclear factor NR2F2 (also known as COUP-TFII), dictates LEC differentiation from the CV [24, 25]. In addition, GATA2, HHEX, and PROX1 itself have recently been shown to up-regulate PROX1 expression [26-29]. The newly specified LECs subsequently bud from the CV and migrate (E10.0-E11.5) in a dorsolateral fashion to form lymph sacs and, thereby establish the functional lymphatic vessels. VEGFC-induced VEGFR3 signaling is the major driver of lymphangiogenesis in vertebrates. Interestingly, in addition to the regulation of LEC sprouting, VEGFR3 signaling also controls LEC progenitor homeostasis by maintaining PROX1 expression levels in a positive feedback loop [22]. In zebrafish, Vegfc/Vegfr3 signaling increases Prox1$^+$ LEC progenitors in the axis vasculature [30, 31]. Conversely, mice deficient in either CCBE1 (a critical matrix protein regulating VEGFC bioavailability), VEGFC, or VEGFR3 reduce PROX1-positive LECs in the CV [23, 32, 33].

The developmental venous origin of the lymphatic endothelium and the requirement for VEGFC/VEGFR3 signaling in lymphangiogenesis are highly conserved from zebrafish to mice to

humans [21, 34]. In zebrafish, from 30 to 32 hours post fertilization (hpf), bi-potential precursor cells in the posterior cardinal veins (PCV) express Prox1 and undergo a Vegfc/Vegfr3-dependent cell division to generate lymphatic and venous daughter cells. In response to the Vegfc cue, the daughter cells on the PCV progressively acquire the LEC fate at 36 hpf; among these, approximately half form parachordal LECs (PL) at the horizontal myoseptum by 48 hpf [31, 35]. These PLs subsequently migrate ventrally and dorsally along the arterial intersegmental vessels (ISVs) at ~60 hpf [35], to form the thoracic duct (TD), intersegmental lymphatic vessels, and dorsal longitudinal lymphatic vessels (DLLV) [21]. Wnt5b has been reported to function upstream of Prox1 to regulate proper lymphatic specification [16]. Nevertheless, the dynamics of LEC fate determination and the molecular mechanism of this process remain to be further understood.

We have demonstrated that the secreted protein AIBP limits angiogenesis in a non-cell autonomous fashion. Mechanistically, extracellular AIBP binds to plasma membrane of ECs, accelerates cholesterol efflux from ECs to high-density lipoprotein (HDL) and reduces lipid raft/caveolae abundance, which in turn disrupts VEGFR2 signaling, thereby restricting angiogenesis [36, 37]. Lymphatic vessels are structurally and functionally related to blood vessels. Many genes that are required for angiogenesis, such as VEGFR3, FGF, Dll4-Notch, angiopoietin-Tie2, Ephrin B2, and TGFβ family member ALK1, Epsin, and others, also function in lymphangiogenesis [5, 38-48]. Thus, we sought to explore the role AIBP-regulated cholesterol metabolism in lymphangiogenesis. In contrast to its role in angiogenesis, our studies reveal an unexpected role of AIBP in promoting lymphangiogenesis. Mechanistically, AIBP augments VEGFC-engaged VEFGR3 signaling in a caveolin 1 (CAV-1)-dependent fashion. Our findings provide a new class of potential therapeutic targets for the treatment of lymphatic disease.

Results

Depletion of Aibp2 impairs lymphangiogenesis in zebrafish

We investigated lymphatic vessel formation in the recently generated Aibp2 knockout zebrafish[49]. The *apoa1bp2*$^{-/-}$ zebrafish were crossbred with *fli1a:egfp* zebrafish that express EGFP in the both the lymphatic and blood ECs [35, 50], generating *apoa1bp2*$^{-/-}$; *fli1a:egfp*. The TD is the first functional lymphatic vessel formed in the zebrafish trunk, situated between the dorsal aorta (DA) and PCV. At 5 days post fertilization (dpf), control siblings have a clearly demarcated TD running between the DA and PCV, whereas ~90% of *apoa1bp2*$^{-/-}$ embryos exhibit ≤30% length of normal TD. Notably, ~80% of mutants show a complete loss of this primary lymphatic vessel (Figure. 1A and B). Since the TD arises from the migration of PLs from the horizontal myoseptum, we assessed the development of PLs in the presence or absence of Aibp2. As illustrated in Figure. 1C and D at 48 hpf, the PL string was normally formed in control embryos, but was completely abolished in ~82% of *apoa1bp2*$^{-/-}$ animals and formed in a few segments (0-30%) in ~8% of animals. Similar developmental defects of TD and PLs were observed by morpholino antisense oligo (MO)-mediated *apoa1bp2* knockdown, which were restored to a large extent by co-injection of *apoa1bp2* mRNA (Figures. S1A-S1C). Impaired TD formation can also be found in *apoa1bp2*$^{-/-}$; *lyve1:Dsred* zebrafish (Figures S1F and S1G), which express DsRed in the lymphatic and venous ECs [51]. Taken together, our data suggest that Aibp2 is required for lymphatic vessel development.

AIBP enhances LEC lineage specification in zebrafish and in the mouse embryonic stem cells (mESCs) to LEC differentiation model

The defects in PL formation motivated us to explore whether Aibp2 has any effect on lymphatic progenitor specification. We performed immunostaining of Prox1 at 36 hpf because Prox1 is the master transcription factor that dictates LEC fate specification [28, 30, 31]. In control siblings, ~ 3 of Prox1-positive LEC progenitors per 6 segments were found in the PCV. By contrast, Aibp2

knockout markedly reduced the number of lymphatic precursors to ~1 (Figure. 1E and F), suggesting that Aibp2 regulates the development of lymphatic progenitors. We also analyzed the lymphatic vessel formation in embryos injected with *apoa1bp2* MO at 36 hpf. Reduced numbers of LEC progenitors in Aibp2 morphants corroborates the Aibp2 effect on lymphatic progenitor specification (Figures S1D and S1E).

We next determined whether the role of AIBP in lymphatic progenitor specification is evolutionarily conserved. Mouse embryoid bodies (mEBs) prepared from mESCs can be differentiated into derivatives of ectodermal, mesodermal, and endodermal tissues and recapitulate certain developmental processes [52]. The LECs emerge from the mesoderm. We prepared mEBs and assessed LEC generation in a differentiation medium containing BMP4 and bFGF followed by additional supplement on day 3 through day 7 with recombinant VEGFA and VEGFC in combination or with AIBP alone (Figure. 1G). From day 0 onwards during differentiation, LECs were identified by the expression of PECAM1, LYVE1 and PROX1, as previously reported [53]. Compared with control cells, VEGFA and VEGFC co-treatment increased both the mRNA and protein expression levels of the LEC-associated markers, LYVE1 and PROX1, at day 5 and day 7 of differentiation (Figures 1H-1K). Surprisingly, AIBP alone strikingly increased LEC progenitor specification as evidenced by robust expression of the LEC markers (Figures 1H-1K), comparable to the effect of VEGFA/C co-administration. A greater percentage of $PECAM^{+}/LYVE1^{+}$ LEC population was detected by FACS analysis at day 7 of LEC differentiation in the presence of AIBP or VEGFA/C (Figures S2A and S2B). These results suggest that AIBP regulation of LEC fate is conserved across evolution.

Aibp2-mediated cholesterol efflux is essential for proper lymphangiogenesis

Our previous studies document that AIBP accelerates cholesterol efflux from ECs [37]. Thus, we first measured free cholesterol levels in *apoa1bp2*$^{-/-}$ embryos. Indeed, Aibp2 depletion significantly

increases free cholesterol content in *apoa1bp2*$^{-/-}$ embryos (Figure 2A). We then treated *apoa1bp2*$^{-/-}$ animals with atorvastatin, a cholesterol-lowering drug, and assessed the attendant effect on lymphangiogenesis. We found that ~93% of *apoa1bp2*$^{-/-}$ embryos displayed ≤50% TD formation and, within this population, ~80% of the embryos lacked the TD. In contrast, atorvastatin treatment substantially reduced the percentage of *apoa1bp2*$^{-/-}$ mutants with incomplete TD development, suggesting that atorvastatin-mediated reduction of cell cholesterol content rescues lymphatic vessel formation (Figures 2B and 2C). In addition, we overexpressed ApoA1, the major protein constituent of HDL, in *apoa1bp2* knockout zebrafish. Similarly, enforced human ApoA1 expression corrected TD formation in *apoa1bp2* knockout animals, as evidenced by the fact that ~76% of *apoa1bp2*$^{-/-}$ zebrafish receiving *APOA1* mRNA show rescued TD development (Figures 2D and 2E). These results indicate that Aibp2 regulates lymphatic vessel formation through cholesterol metabolism.

AIBP-mediated cholesterol efflux disrupts caveolae and enhances VEGFC/VEGFR3 signaling in human LECs

CAV-1, a structural protein organizing the formation of caveolae, binds cholesterol directly, thereby forming cholesterol-rich microdomains, which provide a platform to facilitate membrane-anchored receptor signaling [54, 55]. CAV-1 ablation in mice eliminates caveolae [56, 57]. Both the expression of CAV-1 and the formation of caveolae are dependent on cellular cholesterol levels. In many cases, CAV-1 deficiency alters plasma membrane receptor signaling competence through disruption of caveolae [58-60].

Following LEC specification from the venous ECs, VEGFR3 signaling is required for the maintenance of the LEC progenitor fate, as well as LEC proliferation and migration [31]. CAV-1 in caveolae was reported to repress VEGFR3 activity in the ECs [61]. We postulate that AIBP-mediated cholesterol efflux regulates lymphangiogenesis through CAV-1-dependent

VEGFC/VEGFR3 signaling. As shown in Figures 3A and 3B, compared with VEGFC treatment in human LECs (hLECs), methyl beta cyclodextrin (MβCD)-mediated cholesterol depletion profoundly increased VEGFC-induced VEGFR3 activation, suggesting that caveolae abundance and associated CAV-1 bioavailability inhibit VEGFR3 signaling. Given that AIBP-mediated cholesterol efflux disrupts caveolae, we tested whether AIBP exerts its effect on CAV-1-regulated VEGFC/VEGFR3 signaling via modulation of caveolae. We performed detergent-free, discontinuous gradient ultracentrifugation analysis of hLECs that were pre-incubated with control media, AIBP, HDL_3, or their combination. As anticipated, VEGFR3 was present in the caveolar fractions that were positive for CAV-1 (Figure 3C). AIBP and HDL_3 treatment in concert, which disrupts caveolae, decreased CAV-1 localization in the caveolar fraction and induced VEGFR3 redistribution from the caveolar to the non-caveolar domains (Figure 3C). To further investigate the effect of AIBP-mediated cholesterol efflux on VEGFR3 activation, we treated hLECs with AIBP, HDL_3, or their combination, followed by VEGFC stimulation. We found that AIBP or HDL_3 alone did not significantly affect VEGFC-induced activation of AKT and ERK, the two downstream effector kinases. However, AIBP and HDL_3 in combination, in analogy to treatment with MβCD (Figure 3B), facilitated VEGFC-induced VEGFR3 activation, as shown by markedly increased phosphorylation of AKT and ERK (Figures 3D-3F). These results suggest that AIBP-mediated cholesterol efflux disrupts plasma membrane caveolae, thereby facilitating lymphangiogenesis by augmenting VEGFR3 activation.

Disrupted CAV-1 and VEGFR3 interaction augments VEGFR3 signaling in hLECs.

Whereas Cav-1 is a core component of caveolae, it is also a scaffolding protein that provides a spatially restricted platform for proper signaling of cell surface receptors [62]. Cav-1 contains a signaling motif that interacts with a variety of membrane receptors and modulates their activities [63]. We found that VEGFR3 contains such a conserved motif (Figure 4A), implying possible

regulation of its signaling by CAV-1. We thus generated a VEGFR3 mutant VEGFR3^{AAA} that lacks the three conserved amino acids in the hypothetical CAV-1 binding domain. We overexpressed EGFP, VEGFR3, or VEGFR3^{AAA} in hLECs using lentivirus-mediated gene transfer and examined Cav-1/VEGFR3 interaction. As illustrated in Figure 4B, wild-type VEGFR3, but not VEGFR3^{AAA}, binds CAV-1 in hLECs.

To test the effect of the VEGFR3^{AAA} mutant on VEGFR3 signaling, we ectopically expressed EGFP, VEGFR3 and VEGFR3^{AAA} in hLECs using lentivirus-mediated transfection, followed by stimulation with VEGFC, and assessed VEGFR3 activation. The results show that the triple Ala point mutations, which disrupt its interaction with CAV-1 (Figure 4B), result in potent VEGFC-induced VEGFR3 phosphorylation as well as AKT and ERK activation when compared to wild-type VEGFR3 (Figures 4C-4F). Taken together, our data suggest that AIBP-mediated cholesterol efflux disrupts plasma membrane caveolae and mitigates CAV-1-mediated inhibition of VEGFR3 signaling in LEC.

Cav-1 regulates LEC progenitor development and loss of Cav-1 rescues defective lymphangiogenesis in Aibp2-deficient zebrafish

To explore the role of Cav-1 in lymphatic vessel formation, we generated *cav-1*$^{-/-}$ mutant zebrafish (Figures S3A-S3C), in which Western blot analysis revealed the absence of Cav-1 protein (Figure S3D). Morphologically, Cav-1 null zebrafish are comparable to control animals from 6 hpf to 5 dpf (Figure. S3E). Interestingly, Cav-1 knockout zebrafish showed greater numbers of Prox1 labeled LEC progenitors at 36 hpf (Figures 5A and 5B). However, TD formation appeared normal in these animals (Figures 5C and 5D). Cav-1 depletion or overexpression resulted in profoundly increased or reduced expression of lymphatics-associated genes at 96 hpf, respectively (Figures S4A and S4B).

To determine whether Vegfr3 mediates the cholesterol-associated Cav-1 effect on lymphatic development in zebrafish, we generated a knock-in zebrafish Vegfr3 mutant in which the Cav-1 binding site of Vegfr3 (W1106A/F1108A/W1113A) was replaced with the non-binding domain (Figures S5A and S5B). The control wild type Vegfr3 animals were generated in a similar fashion. Both mutant lines were crossed to *fli1a:DsRed* to generate *fli1a:DsRed; flt4*$^{+/\Delta Cav\text{-}1}$ or *fli1a:DsRed; flt4*$^{+/wt}$. Confocal imaging of TD formation at 4 dpf reveals increased TD length in the *fli1a:DsRed; flt4*$^{+/\Delta Cav\text{-}1}$ compared to the control *fli1a:DsRed; flt4*$^{+/wt}$ (Figures 5E and 5F). Thus, our data show that Cav-1 suppresses lymphatic progenitor development and lymphangiogenesis in zebrafish.

We have shown that Aibp2 knockout increases free cholesterol content (Figure 2A), which presumably increases caveolae content, as cholesterol is enriched in the caveolae [64]. Given that CAV-1-organized caveolae negatively regulate VEGFR3 signaling [61], we examined the effect of Cav-1 deletion on lymphangiogenesis in Aibp2-deficient animals. As expected, absence of Cav-1 rescued impaired lymphatic progenitor development in Aibp2 knockdown animals as revealed by recovered Prox1 staining (Figures 5A and 5B). Consistent with this rescue effect, defective TD formation was restored in the Cav-1- and Aibp2- double deficient animals (Figures 5C and 5D). The data suggest that Cav-1 functions downstream of Aibp2-mediated cholesterol efflux.

AIBP-mediated cholesterol efflux promotes adult lymphangiogenesis in mice

Since Cav-1 depletion rescues TD development in Aibp2 morphants, we hypothesized that Aibp2, by alleviating Cav-1 repression of Vegfr3, facilitates lymphangiogenesis. We further investigated this mechanism in a murine model, to determine whether this mechanism is evolutionarily conserved. Indeed, loss of CAV-1 [56] significantly augmented tail lymphangiogenesis in P3 neonatal mice, as revealed by LYVE-1 antibody staining of lymphatic vessels in the analogous anatomic location (Figures S6A and S6B). The corneas of adult mice lack lymphatic vasculature [65, 66], thereby providing a widely used model to study injury or growth factor-induced

lymphangiogenesis (Figure 6A). To explore the role of cholesterol efflux in adult lymphangiogenesis, we implanted VEGFC-containing pellets, in the presence or absence of recombinant AIBP and the core protein component of HDL – APOA1 or the CAV-1 blocking peptide (CAV-1 scaffolding domain, CSD), into the corneas of B6 mice. We used ApoA1 in this assay due to technical difficulties in the preparation of HDL pellets. As expected, VEGFC pellet implantation elicited robust lymphangiogenesis (Figure 6B). AIBP and APOA1 in combination or CSD further increased VEGFC-induced lymphangiogenesis (Figures 6B and 6C). Remarkably, VEGFC in combination with AIBP alone exhibited analogously potent pro-lymphangiogenic efficacy in that mice generally contain high plasma levels of HDL cholesterol resulting from APOA1 lipidation (Figures 6B and C). However, no pro-lymphangiogenic effect was found with AIBP/APOA1 or CSD treatment in the absence of VEGFC (Figure S7). Thus, consistent with our studies in zebrafish, AIBP-mediated cholesterol efflux increases lymphangiogenesis in neonatal and adult mice.

AIBP gain-of-function or CAV-1 loss-of-function improves VEGFC-mediated tail lymphedema recovery in mice and reduced AIBP expression is found in the affected epidermis of lymphedema patients

To determine the potential therapeutic significance of the AIBP-CAV-1-VEGFR3 signaling axis, we utilized the murine tail lymphedema model. The circumferential skin was surgically removed to disrupt the lymphatic flow and elicit lymphedema as previously described [5, 67]. We intraperitoneally delivered recombinant VEGFC protein, alone or in combination with recombinant human AIBP, and assessed the recovery from lymphedema. Consistent with corneal lymphangiogenesis, AIBP/VEGFC or CSD/VEGFC co-administration enhanced recovery from lymphedema compared to VEGFC treatment alone at day 14 post-surgery (Figures 7A and 7B). To probe the association of AIBP content with lymphatic vessel dysfunction, we examined AIBP

expression in human skin specimens derived from 7 subjects. We obtained paired cutaneous normal and lymphedematous biopsy specimens from each of these individuals. Immunohistochemical staining of AIBP showed that it is robustly expressed in the epidermis and the sweat glands (Figure 7C). Interestingly, in human lymphedema, AIBP expression is mildly but significantly reduced in the epidermis but not in the dermis or sweat glands, when compared to the paired normal cutaneous specimens (Figures 7C-7F). The comparable expression in the dermis and sweat gland excludes the possibility that tissue swelling dilutes AIBP content in the epidermis of lymphedema biopsy samples. The observed abnormality in the lymphedematous epidermis suggests that reduced AIBP expression is associated with impairment of cutaneous lymphatic function.

Discussion

In this paper, we reveal a novel molecular mechanism underlying lymphatic development, in which AIBP-mediated cholesterol efflux disrupts caveolae and, as a consequence, reduces CAV-1 bioavailability, thereby mitigating the CAV-1 inhibition of VEGFR3 activation and augmenting lymphatic fate commitment and lymphangiogenesis. Our mechanistic study of AIBP-regulated lymphangiogenesis may have the capacity to foster the development of new therapies for the diseases associated with lymphatic dysfunction.

Opposing roles of AIBP in angiogenesis and lymphangiogenesis

Our previous studies have shown that AIBP-mediated cholesterol efflux disrupts lipid rafts/caveolae, which results in restricted angiogenesis by two mechanisms: 1) it impedes rafts/caveolae-anchored proangiogenic VEGFR2 clustering, endocytosis and signaling, thereby restricting angiogenesis [37], and 2) it translocates γ-secretase from lipid rafts/caveolae to the non-raft/caveolar domain, facilitating the cleavage of NOTCH1 receptor and augmenting anti-

angiogenic NOTCH1 signaling [36]. Recently, we demonstrated that AIBP instructs hematopoietic stem and progenitor cell specification in development through activation of SREBP2, which in turn transactivates NOTCH1 for hematopoiesis [49]. Here, we show that AIBP increases lymphangiogenesis and instructs LEC progenitor specification. At the molecular level, AIBP-mediated cholesterol efflux attenuates the inhibitory effect of CAV-1 on VEGFR3 signaling. Thus, disruption of CAV-1 and VEGFR3 binding augments VEGFR3 signaling and LEC progenitor development and lymphangiogenesis. Although LECs are derived from blood ECs (BEC), their functions and molecular identifications differ. The fundamental differences between BECs and LECs may contribute to the disparate effects of AIBP on angiogenesis and lymphangiogenesis.

It is not unprecedent that one protein may have the opposing effects on angiogenesis and lymphangiogenesis. For instance, RhoB ablation augments lymphangiogenesis but impairs angiogenesis in the cutaneous wound healing model [68]. Although Notch signaling limits angiogenesis [69-71], Notch has been reported to inhibit or augment lymphangiogenesis in a context-dependent fashion [38, 39, 72, 73]. In addition, a recent study also documents the contrary role of two angiostatic components, DLL4 and S1PR1, in lymphangiogenesis [74].

AIBP-mediated CAV-1-dependent regulation of VEGFR3 signaling and lymphangiogenesis

Lymphatic vessel formation requires LEC fate commitment and subsequent sprouting. LEC fate acquisition, LEC sprouting from the embryonic CV, and dorsolateral migration under the control of VEGFC/VEGFR3/PROX1 signaling axis is highly conserved [27]. Restricted expression of PROX1 protein dictates LEC identity , which is critical for future LECs to migrate out of the PCV [28]. AIBP is evolutionarily conserved from zebrafish to human. Zebrafish have two *apoa1bp* genes that encode Aibp1 and Aibp2 proteins, and Aibp2 demonstrates functional properties resembling those of human AIBP [37]. Although the degree of phenotypic severity varies, most of the Aibp2 mutants show a partial or complete loss of PLs in the horizontal myoseptum region and, thus, lack

large portion or all of the TD arising from PLs. Furthermore, these defects are likely attributed to a failure of LEC lineage commitment, as Aibp2 loss-of-function impairs lymphatic precursor specification (Figures 1E and 1F).

A positive feedback loop between VEGFR3 and PROX1 is necessary to maintain the identity of LEC progenitors in mice and zebrafish [22, 31]. CAV-1 has been reported to inhibit VEGFR3 signaling in ECs [61]. Our studies show that Cav-1 knockdown or overexpression in zebrafish increases or decreases expression of lymphatic genes, respectively. Moreover, loss of Cav-1 strongly enhances lymphatic progenitor specification and rescues impaired lymphangiogenesis. Despite increased number of LEC progenitors, the TD formation appears normal in Cav-1 null zebrafish (Figures 5C and 5D). Indeed, there are considerable variations in the number of LECs required to form a complete TD, as previously reported [31].

AIBP augmentation or CAV-1 disruption facilitates VEGFC function in murine tail lymphedema (Figures 7A and 7B), which further corroborates the pro-lymphangiogenic role of the AIBP-CAV-1-VEGFR3 axis. This treatment regimen has theoretical superiority to isolated VEGFC augmentation, because VEGFC augments neovascularization and vascular leakage [75]. In contrast, AIBP or CAV-1 inhibition confers an angiostatic effect [36, 37, 76].

Conserved role of AIBP in the regulation of LEC fate and lymphangiogenesis

In the mESC-to-LEC differentiation model, we found that recombinant AIBP incubation displays a remarkable effect on the LEC specification arising from mesodermal origin. Given that AIBP alone has no observable effect on VEGFR3 phosphorylation, this AIBP effect on LEC fate commitment is likely due to a synergistic effect of AIBP and increased VEGFR signaling in the induced mesoderm [77, 78]. Although AIBP is unlikely to initiate ligand-independent signaling, it fine-tunes VEGFC/VEGFR3 signaling.

Earlier studies support the fact that LECs emerge from venous origin [2, 15, 16]. However, other mechanisms of lymphatic vessel formation have been reported recently, such as in the zebrafish facial lymphatics [18], and in murine dermal and cardiac lymphatic vessel formation [19, 79], and in zebrafish brain [17, 20]. The Aibp2 effect on lymphatic vessel formation is blunted at later developmental stages in zebrafish, and we also did not detect a significant difference in tail lymphangiogenesis between AIBP knockout neonatal mice and control littermates (data not shown), which could be due to the rescue effect of non-venous origin-derived lymphangiogenesis.

It often takes years to develop secondary lymphedema, an acquired damage to the lymphatic system occasioned by surgical disruption, radiotherapy, or infection [10, 80]. Genetic studies suggest that small changes in an array of lymphangiogenic genes, in the absence of a single dominant mutation, may precipitate secondary lymphedema [81]. Our AIBP staining of paired human normal/lymphedema cutaneous biopsy specimens revealed that AIBP expression is significantly reduced in the epidermis in the setting of human lymphedema when compared to the paired normal counterpart specimens. Whereas it is a mild change, this may be indicative of a general attenuation of lymphangiogenic potential in the lymphedematous tissues.

Methods

Zebrafish husbandry

All the wild-type AB and transgenic Zebrafish lines were maintained as previously described [49] and in accordance with Houston Methodist Research Institute Animal Care and Use Committee (IACUC) regulations and under the appropriate project protocols.

MO and mRNA injections

Morpholino antisense oligos (MOs) were synthesized by Gene Tools. The following MOs were used in this study 1) control: 5'- CCTCTTACCTCAGTTACAATTTATA-3', and 2) *apoa1bp2* (NCBI

Gene ID: 557840): 5'-GTGGTTCATCTTGATTTATTCGGC-3'[49]. The working concentrations of control and *aopa1bp2* MOs were 0.2 mM and 0.1 mM, respectively. Equal volume of *aopa1bp2* MO (0.1 mM) and *aopoa1bp2* mRNA (200 ng/μl) were mixed to perform the rescue assays. The working concentration of human *APOA1* mRNA was 100 ng/μl. One nl of MO, mRNA or the combination of MO with mRNA were injected into one-cell stage embryo using the microinjector FemtoJet® 4i (Eppendorf).

CRISPR/Cas9-mediated gene knockout mutant

The CRISPR/Cas9-mediated gene knockout technique was performed as previously described [49, 82]. Briefly, the target sequence of caveolin 1 (Cav-1, NCBI Gene ID: 323695) was 5'-GACGTGATCGCCGAGCCTGC-3'. The guide-RNA (gRNA) sequence was subcloned into pT7-gRNA vector and gRNA was synthesized using HiScribeTM T7 Quick High Yield RNA Synthesis (New England Biolabs). The pCS2-nCas9n was linearized using NotI and Cas9 mRNA was synthesized using mMESSAGE mMACHINE SP6 Kit (Invitrogen). Twenty-five ng/μl gRNA and 200 ng/μl Cas9 mRNA were mixed and injected into one-cell stage wild type embryos. The found zebrafish were raised to adult. Following genotype verification using DNA sequencing.

Chemical treatments

For atorvastatin (PZ0001, Sigma) treatment, embryos were treated with 1 μM atorvastatin from 6 to 120 hpf. All control embryos were incubated with equal amount of ethanol at the indicated time points.

Cell culture

Human dermal lymphatic microvascular endothelial cells (hLECs) were cultured in Endothelial Cell Medium. Methyl-β-cyclodextrin was prepared in serum-free ECM medium with a working

concentration of 10 mM. HDL_3 isolation was performed as previous described [36]. The hLECs were pretreated with 200 ng/ml AIBP protein, 100 μg/ml HDL_3, or the combination of AIBP with HDL_3 for 4 hours, washed with PBS, and followed by incubation with VEGFC (100 ng/ml) in prewarmed serum-free ECM medium for 20 min.

Lentivirus infection

The hLECs were transduced with the third generation lentiviral system as previous described . After the cells were infected with human VEGFR3, $VEGFR3^{AAA}$ or CAV1 overexpression Lenti-virus for 96 hours, cells were subjected to puromycin (5 μg/ml) selection to generate pool cells stably expressing the transduced genes.

Quantitative PCR

The qPCR was performed as previously described [49] . The gene information and the primers used in this study were listed in the STAR★METHODS.

Western blot and Immunoprecipitation

Zebrafish or hLECs were lysed on ice with the RIPA buffer (Pierce) and western blotting was performed as previously described [49]. Immunoprecipitation was performed using the Pierce Classic Magnetic IP/Co-IP Kit following the manufacturer's instruction.

Mouse embryonic stem cell (mESC) culture

The mESCs were cultured in feeder- and serum-free environment using ESGRO®-2i medium supplemented with leukemia inhibitory factor (LIF), GSK3β inhibitor and MEK1/2 inhibitor according to the manufacturer's instruction. Briefly, T25 flask was coated with 0.1% gelatin solution for 30 min at room temperature, and then 1×10^6 cells were plated onto gelatinized T25

flask in ESGRO®-2i medium and incubated at 37 °C with 5% CO_2. The media were changed daily and mESCs were sub-cultured at a ratio of 1:5 when cells reached 60-90% confluence.

Lymphatic endothelial cell (LEC) differentiation

The mESCs differentiation to the endothelial lineage was performed as previously described with the following modifications [83]. Briefly, mESCs were seeded onto collagen IV-coated plates and maintained in LEC differentiation medium supplemented with 2 ng/ml BMP4, 10 ng/ml bFGF, 50 ng/ml VEGFA and 50 ng/ml VEGFC for 7 days. Differentiated cells were collected on days 3, 5 and 7 for qPCR, western blot, or FACS analysis.

Fluorescence Activated Cell Sorting (FACS) analysis

Cells were dissociated using enzyme-free Hanks' Balanced Salt Solution, resuspended in 1× DPBS supplemented with 2% heat-inactivated FBS. Cells were then stained with APC anti-CD31 antibody, Alexa Fluor 488 conjugated LYVE1 Monoclonal Antibody and DAPI, and analyzed by BD LSR II flow cytometer. Data were analyzed using the FlowJo software.

VEGFR3 site-direct mutation

VEGFR3 mutation was generated using a PCR-based direct site mutation strategy. Briefly, the plasmid containing wild type VEGFR3 was amplified using primer pair $VEGFR3^{AAA}$-F (5'-ACGCAGAGTGACGTGGCGTCCGCTGGGGTGCTTCTCGCGGAGATCTTCTCTCTGGGGGC C-3') and $VEGFR3^{AAA}$-R (5'-AGAGAGAAGATCTCCGCGAGAAGCACCCCAGCGGACGCCACGTCACTCTGCGTGGTGTA C-3'). The PCR program was 95 °C for 2 min, 18 cycles of 95 °C for 30 s, 68 °C for 1 min per kilobase of plasmid length, then 68 °C for 7 min and hold at 4°C. One μl DpnI was added to the PCR products to disrupt the plasmid template and incubated at 37°C for 2 hours, and then 5 μl

PCR products were transformed into stbl3 competent cells. The resulting clones were selected, plasmid extracted, and DNA sequenced. The one with expected mutation was used for subsequent experiments.

Prox1 staining

Zebrafish larvae at 36 hpf were fixed in 4% paraformaldehyde for 2 hr at room temperature. Following fixation, larvae were washed with PBS, dehydrated through 25%, 50%, 70% and 100% methanol/PBS series and stored at –20 °C in 100% methanol for later usage. Before usage, larvae were rehydrated through 75%, 50% and 25% methanol/PBS series, washed with PBS/0.1% Tween (PBST), and permeabilized in pre-chilled acetone for 20 min. The resulting animals were then washed with PBST and blocked in 10% BSA/PBST overnight at 4 °C. Following incubation with Prox1 antibody and GFP antibody for 3 days at 4°C, and after proper wash with PBST, the larvae were incubated overnight at 4°C in dark with secondary antibody diluted in 1% BSA/PBST. Following extensive PBST wash, the immunostained animals were imaged using Olympus FV 3000 confocal microscope.

Immunohistochemistry (IHC)

AIBP antibody were generated in rabbits using tag-free recombinant human AIBP proteins. AIBP antibody was subsequently purified from the rabbit antiserum using affinity purification, where AIBP antigen column was prepare by covalently conjugating recombinant AIBP to the amine-reactive, beaded-agarose resin.

The 5 μm human specimens were deparaffinized, and rehydrated serially through xylene, 100%, 80%, and 70% ethanol, and finally rinsed in Milli-Q water. The resulting sections were subjected to antigen recovery by immersing in 100°C citrate buffer pH6.0 for 10 min. An incubation with 3% hydrogen peroxide was then applied at room temperate for additional 10 min

to eliminate the endogenous peroxidase activity. Following rinsing in TBST, the slides were further washed and blocked in TBST with 1% BSA. The slides were incubated with AIBP antibody for 1 hr at room temperature. Following proper TBST wash, the slides were sequentially incubated with biotinylated anti-rabbit (1:200) and Avidin conjugated alkaline phosphatase for 30 minutes (1:1,000) at room temperature. AP blue substrate mixture was administered for final color development (15-30 min). The slides were finally mounted in aqueous mounting medium.

Mouse cornea lymphangiogenesis

VEGFC pellet preparation and implantation were carried out as previously described with minor modifications [48, 65]. Briefly, pellets containing recombinant VEGFC (5 mg/ml), AIBP (10 mg/ml) in combination with apoA-1 (15 mg/ml), CAV-1 scaffolding domain (CSD; 5 mg/ml), VEGFC with AIBP and ApoA1 or with CSD were prepared by mixing with 10% sucralfate solution (w/v in PBS) and 12% poly-HEMA (w/v in ethanol). The aforementioned components were mixed as following: 5 µl of poly-HEMA, 1 µl of sucralfate, 2 µl VEGFC, 2 µl AIBP, 2 µl APOA1, 2 µl CSD, and the final volume adjusted to 10 µl with PBS. The mixture droplet was put on PARAFILM, UV irradiated for 15 minutes, and air-dried in the cell culture hood. Dried pellets were used immediately or stored at 4 °C before usage.

The mouse was anesthetized with isoflurane, and one drop of 0.5% proparacaine HCl was applied to the cornea. Five minutes later, one mouse eye was properly oriented under a dissection microscope. A gentle cut was made with a von Graefe cataract knife from the center of the cornea, and a pocket of ~ 1.5 – 2 mm^2 size was generated by inserting the knife toward corneal limbus, with a few gentle waggles inside. The pellets were then inserted into the cornea pocket using forceps and von Graefe cataract knife, with the pellet flattened to secure the implantation. The ophthalmic antibiotic ointment was applied topically to the injured eye. Following 10 days of pellet implantation, the cornea was dissected and washed in PBS for later processing.

Dissection of the tail skin of neonatal mice

After euthanization, the tails of *Cav1*$^{-/-}$ or littermate control at P3 were dissected, with the tail tips cut off. The tail bones and extra connective tissues were then manually removed. Tails were incubated in 20 mM EDTA/PBS overnight at 4°C to facilitate dermis isolation. The dissected dermis was washed with PBS for subsequent immunostaining as described below.

Immuno-fluorescence (IF) staining of mouse cornea and tail skin

For IF staining, cornea and tail skin were fixed in 4% paraformaldehyde for 2 hr at room temperature. Subsequently, samples were washed 5 times with 0.05% tween/PBS (0.05% PBS-TW) and blocked with the blocking buffer (1% goat or donkey serum, 1% BSA, and 0.5% Triton X-100 in PBS) for 3-4 hr at room temperature. Samples were incubated with LYVE-1 antibody (1:1000) and CD31 antibody (1:1000) diluted in the blocking solution for 2 days and with secondary antibodies (1:1000) overnight at 4°C following proper wash with 0.5% Triton X-100/PBS (0.5% PBS-TX). The immunostained tissues were flat-mounted in the mounting medium and stored at 4 °C before imaging.

Confocal imaging and image quantification

Flatmounted tissues were imaged using Nikon A1 confocal microscope. Auto-stitching function was applied to generate the whole cornea image. Z-stacked images were maxi-projected and processed using Image J. Color balance and threshold were adjusted using the same threshold for image quantification.

For quantification of tail lymphatic vessels, images were converted to binary image by applying “Erode” or “Dilate” options as exampled (https://imagej.nih.gov/ij/docs/menus/process.html), and images were skeletonized. Skeleton length was quantified, and pixel value was converted to micrometer (μm).

For quantification of cornea lymphatic vessel and blood vessel, region of interest (ROI) on each image were chosen based on the location of the VEGFC containing pellets. ROI images were processed using Image J to quantify percentage of lymphatic vessel or blood vessel coverage as reported [6].

Statistical analysis

Statistical comparisons between two groups were analyzed using Student *t* test. One-way ANOVA was used to compare the means of multiple groups. Data were expressed as the mean±SD if n<5 or as the mean±SEM if n≥5. *P*<0.05 was considered statistically significant. *, p<0.05; **, p<0.01; ***, p<0.001; ***, p<0.0001.

Acknowledgements

We thank Dr. Henry Pownall (HMRI) for providing purified human APOA1 protein. We thank Drs John P. Cooke (HMRI) and Eva Sevick (UT-HSC) for their help and suggestions on this project. This project was supported by grants (NIH HL132155, AHA 16BGIA27790081, AHA 18TPA34250009, and HMRI startup fund) to L.F., by grant (HL093242, HL130845, and HL133216) to H.C, AHA (17POST33410671) to X.Y, and AHA (18CDA34110132) to JK, Grants (AHA 19CDA34760260 and a grant from the Oklahoma Center for Adult Stem Cell Research) to P. Y.

Author contributions

XY and JK designed the experiments, performed most of the experiments and analyzed the data. XY generated the majority of the data in zebrafish and in cell culture models, and JK mainly performed the studies in mice and using human specimens. YL and PA initiated the tail lymphedema study for this project in the Chen laboratory. HC and QG helped on some of the

experiment design, experimentation, and data analysis. QY prepared HDL_3 and recombinant AIBP. PY, JA, PC and HC provided critical suggestions, experimental materials, and technical guidance for this project. SGR provided constructive suggestions and tissues of lymphedema patients and participated in manuscript preparation. LF conceived the project, designed experiments, and supervised the studies. XY and LF wrote the manuscript with input from the co-authors.

Competing interests
The authors declare no competing financial interest.

References

1. Schulte-Merker, S., Sabine, A. & Petrova, T.V. Lymphatic vascular morphogenesis in development, physiology, and disease. *J Cell Biol* **193**, 607-618 (2011).

2. Escobedo, N. & Oliver, G. The Lymphatic Vasculature: Its Role in Adipose Metabolism and Obesity. *Cell Metab* **26**, 598-609 (2017).

3. Alitalo, K., Tammela, T. & Petrova, T.V. Lymphangiogenesis in development and human disease. *Nature* **438**, 946-953 (2005).

4. Sasso, M.S. *et al.* Lymphangiogenesis-inducing vaccines elicit potent and long-lasting T cell immunity against melanomas. *Sci Adv* **7** (2021).

5. Wu, H. *et al.* Epsin deficiency promotes lymphangiogenesis through regulation of VEGFR3 degradation in diabetes. *J Clin Invest* **128**, 4025-4043 (2018).

6. Ma, Q. *et al.* Unexpected contribution of lymphatic vessels to promotion of distant metastatic tumor spread. *Sci Adv* **4**, eaat4758 (2018).

7. Naxerova, K. *et al.* Origins of lymphatic and distant metastases in human colorectal cancer. *Science* **357**, 55-60 (2017).

8. Lim, H.Y. *et al.* Lymphatic vessels are essential for the removal of cholesterol from peripheral tissues by SR-BI-mediated transport of HDL. *Cell Metab* **17**, 671-684 (2013).

9. Martel, C. *et al.* Lymphatic vasculature mediates macrophage reverse cholesterol transport in mice. *J Clin Invest* **123**, 1571-1579 (2013).

10. Brakenhielm, E. & Alitalo, K. Cardiac lymphatics in health and disease. *Nat Rev Cardiol* **16**, 56-68 (2019).

11. Zhang, F. *et al.* Lacteal junction zippering protects against diet-induced obesity. *Science* **361**, 599-603 (2018).

12. Alitalo, K. The lymphatic vasculature in disease. *Nat Med* **17**, 1371-1380 (2011).

13. Secker, G.A. & Harvey, N.L. VEGFR signaling during lymphatic vascular development: From progenitor cells to functional vessels. *Dev Dyn* **244**, 323-331 (2015).

14. Bautch, V.L. & Caron, K.M. Blood and lymphatic vessel formation. *Cold Spring Harb Perspect Biol* **7**, a008268 (2015).

15. Potente, M. & Makinen, T. Vascular heterogeneity and specialization in development and disease. *Nat Rev Mol Cell Biol* **18**, 477-494 (2017).

16. Nicenboim, J. *et al.* Lymphatic vessels arise from specialized angioblasts within a venous niche. *Nature* **522**, 56 (2015).

17. Bower, N.I. *et al.* Mural lymphatic endothelial cells regulate meningeal angiogenesis in the zebrafish. *Nat Neurosci* **20**, 774-783 (2017).

18. Eng, T.C. *et al.* Zebrafish facial lymphatics develop through sequential addition of venous and non-venous progenitors. *EMBO Rep* **20** (2019).

19. Klotz, L. *et al.* Cardiac lymphatics are heterogeneous in origin and respond to injury. *Nature* (2015).

20. Venero Galanternik, M. *et al.* A novel perivascular cell population in the zebrafish brain. *Elife* **6** (2017).

21. Koltowska, K., Betterman, K.L., Harvey, N.L. & Hogan, B.M. Getting out and about: the emergence and morphogenesis of the vertebrate lymphatic vasculature. *Development* **140**, 1857-1870 (2013).

22. Srinivasan, R.S. *et al.* The Prox1–Vegfr3 feedback loop maintains the identity and the number of lymphatic endothelial cell progenitors. *Genes Dev* **28**, 2175-2187 (2014).

23. Karkkainen, M.J. *et al.* Vascular endothelial growth factor C is required for sprouting of the first lymphatic vessels from embryonic veins. *Nat Immunol* **5**, 74-80 (2004).

24. François, M. *et al.* Sox18 induces development of the lymphatic vasculature in mice. *Nature* **456**, 643 (2008).

25. Srinivasan, R.S. *et al.* The nuclear hormone receptor Coup-TFII is required for the initiation and early maintenance of Prox1 expression in lymphatic endothelial cells. *Genes Dev* **24**, 696-707 (2010).

26. Kazenwadel, J. *et al.* GATA2 is required for lymphatic vessel valve development and maintenance. *J Clin Invest* **125**, 2979-2994 (2015).

27. Gauvrit, S. *et al.* HHEX is a transcriptional regulator of the VEGFC/FLT4/PROX1 signaling axis during vascular development. *Nat Commun* **9**, 2704 (2018).

28. Srinivasan, R.S. & Oliver, G. Prox1 dosage controls the number of lymphatic endothelial cell progenitors and the formation of the lymphovenous valves. *Genes Dev* **25**, 2187-2197 (2011).

29. Frye, M. *et al.* Matrix stiffness controls lymphatic vessel formation through regulation of a GATA2-dependent transcriptional program. *Nat Commun* **9**, 1511 (2018).

30. Shin, M. *et al.* Vegfc acts through ERK to induce sprouting and differentiation of trunk lymphatic progenitors. *Development* **143**, 3785-3795 (2016).

31. Koltowska, K. *et al.* Vegfc regulates bipotential precursor division and Prox1 expression to promote lymphatic identity in zebrafish. *Cell Rep* **13**, 1828-1841 (2015).

32. Hägerling, R. *et al.* A novel multistep mechanism for initial lymphangiogenesis in mouse embryos based on ultramicroscopy. *EMBO J* **32**, 629-644 (2013).

33. Bui, H.M. *et al.* Proteolytic activation defines distinct lymphangiogenic mechanisms for VEGFC and VEGFD. *J Clin Invest* **126**, 2167-2180 (2016).

34. Küchler, A.M. *et al.* Development of the zebrafish lymphatic system requires VEGFC signaling. *Curr Biol* **16**, 1244-1248 (2006).

35. Hogan, B.M. *et al.* Ccbe1 is required for embryonic lymphangiogenesis and venous sprouting. *Nat Genet* **41**, 396-398 (2009).

36. Mao, R. *et al.* AIBP Limits Angiogenesis Through gamma-Secretase-Mediated Upregulation of Notch Signaling. *Circ Res* (2017).

37. Fang, L. *et al.* Control of angiogenesis by AIBP-mediated cholesterol efflux. *Nature* **498**, 118-122 (2013).

38. Niessen, K. *et al.* The Notch1-Dll4 signaling pathway regulates mouse postnatal lymphatic development. *Blood* **118**, 1989-1997 (2011).

39. Zheng, W. *et al.* Notch restricts lymphatic vessel sprouting induced by vascular endothelial growth factor. *Blood* **118**, 1154-1162 (2011).

40. Geudens, I. *et al.* Role of delta-like-4/Notch in the formation and wiring of the lymphatic network in zebrafish. *Arterioscler Thromb Vasc Biol* **30**, 1695-1702 (2010).

41. Adams, R.H. *et al.* Roles of ephrinB ligands and EphB receptors in cardiovascular development: demarcation of arterial/venous domains, vascular morphogenesis, and sprouting angiogenesis. *Genes Dev* **13**, 295-306 (1999).

42. Gale, N.W. *et al.* Angiopoietin-2 is required for postnatal angiogenesis and lymphatic patterning, and only the latter role is rescued by Angiopoietin-1. *Dev Cell* **3**, 411-423 (2002).

43. Makinen, T. *et al.* PDZ interaction site in ephrinB2 is required for the remodeling of lymphatic vasculature. *Genes Dev* **19**, 397-410 (2005).

44. Niessen, K., Zhang, G., Ridgway, J.B., Chen, H. & Yan, M. ALK1 signaling regulates early postnatal lymphatic vessel development. *Blood* **115**, 1654-1661 (2010).

45. Seki, T., Yun, J. & Oh, S.P. Arterial endothelium-specific activin receptor-like kinase 1 expression suggests its role in arterialization and vascular remodeling. *Circ Res* **93**, 682-689 (2003).

46. Urness, L.D., Sorensen, L.K. & Li, D.Y. Arteriovenous malformations in mice lacking activin receptor-like kinase-1. *Nat Genet* **26**, 328-331 (2000).

47. Yoshimatsu, Y. *et al.* Bone morphogenetic protein-9 inhibits lymphatic vessel formation via activin receptor-like kinase 1 during development and cancer progression. *Proc Natl Acad Sci U S A* **110**, 18940-18945 (2013).

48. Yu, P. *et al.* FGF-dependent metabolic control of vascular development. *Nature* **545**, 224-228 (2017).

49. Gu, Q. *et al.* AIBP-mediated cholesterol efflux instructs hematopoietic stem and progenitor cell fate. *Science* **363**, 1085-1088 (2019).

50. Lawson, N.D. & Weinstein, B.M. In vivo imaging of embryonic vascular development using transgenic zebrafish. *Dev Biol* **248**, 307-318 (2002).

51. Okuda, K.S. *et al.* lyve1 expression reveals novel lymphatic vessels and new mechanisms for lymphatic vessel development in zebrafish. *Development* **139**, 2381-2391 (2012).

52. Pettinato, G., Wen, X. & Zhang, N. Engineering strategies for the formation of embryoid bodies from human pluripotent stem cells. *Stem Cells Dev* **24**, 1595-1609 (2015).

53. Dunworth, W.P. *et al.* Bone morphogenetic protein 2 signaling negatively modulates lymphatic development in vertebrate embryos. *Circ Res* **114**, 56-66 (2014).

54. Chidlow, J.H., Jr. & Sessa, W.C. Caveolae, caveolins, and cavins: complex control of cellular signalling and inflammation. *Cardiovasc Res* **86**, 219-225 (2010).

55. Razani, B., Woodman, S.E. & Lisanti, M.P. Caveolae: from cell biology to animal physiology. *Pharmacol Rev* **54**, 431-467 (2002).

56. Razani, B. *et al.* Caveolin-1 null mice are viable but show evidence of hyperproliferative and vascular abnormalities. *J Biol Chem* **276**, 38121-38138 (2001).

57. Drab, M. *et al.* Loss of caveolae, vascular dysfunction, and pulmonary defects in caveolin-1 gene-disrupted mice. *Science* **293**, 2449-2452 (2001).

58. Sonveaux, P. *et al.* Caveolin-1 expression is critical for vascular endothelial growth factor-induced ischemic hindlimb collateralization and nitric oxide-mediated angiogenesis. *Circ Res* **95**, 154-161 (2004).

59. Woodman, S.E. *et al.* Caveolin-1 knockout mice show an impaired angiogenic response to exogenous stimuli. *Am J Pathol* **162**, 2059-2068 (2003).

60. Murata, T. *et al.* Reexpression of caveolin-1 in endothelium rescues the vascular, cardiac, and pulmonary defects in global caveolin-1 knockout mice. *J Exp Med* **204**, 2373-2382 (2007).

61. Galvagni, F. *et al.* Vascular endothelial growth factor receptor-3 activity is modulated by its association with caveolin-1 on endothelial membrane. *Biochemistry* **46**, 3998-4005 (2007).

62. Bernatchez, P., Sharma, A., Bauer, P.M., Marin, E. & Sessa, W.C. A noninhibitory mutant of the caveolin-1 scaffolding domain enhances eNOS-derived NO synthesis and vasodilation in mice. *J Clin Invest* **121**, 3747-3755 (2011).

63. Couet, J., Sargiacomo, M. & Lisanti, M.P. Interaction of a receptor tyrosine kinase, EGF-R, with caveolins. Caveolin binding negatively regulates tyrosine and serine/threonine kinase activities. *J Biol Chem* **272**, 30429-30438 (1997).

64. Brown, D.A. & London, E. Structure and function of sphingolipid- and cholesterol-rich membrane rafts. *J Biol Chem* **275**, 17221-17224 (2000).

65. Wong, B.W. *et al.* The role of fatty acid beta-oxidation in lymphangiogenesis. *Nature* **542**, 49-54 (2017).

66. Cao, R. *et al.* Mouse corneal lymphangiogenesis model. *Nat Protoc* **6**, 817-826 (2011).

67. Rutkowski, J.M., Moya, M., Johannes, J., Goldman, J. & Swartz, M.A. Secondary lymphedema in the mouse tail: Lymphatic hyperplasia, VEGF-C upregulation, and the protective role of MMP-9. *Microvasc Res* **72**, 161-171 (2006).

68. Gerald, D. *et al.* RhoB controls coordination of adult angiogenesis and lymphangiogenesis following injury by regulating VEZF1-mediated transcription. *Nat Commun* **4**, 2824 (2013).

69. Hellstrom, M. *et al.* Dll4 signalling through Notch1 regulates formation of tip cells during angiogenesis. *Nature* **445**, 776-780 (2007).

70. Siekmann, A.F. & Lawson, N.D. Notch signalling limits angiogenic cell behaviour in developing zebrafish arteries. *Nature* **445**, 781-784 (2007).

71. Suchting, S. *et al.* The Notch ligand Delta-like 4 negatively regulates endothelial tip cell formation and vessel branching. *Proc Natl Acad Sci U S A* **104**, 3225-3230 (2007).

72. Bernier-Latmani, J. *et al.* DLL4 promotes continuous adult intestinal lacteal regeneration and dietary fat transport. *J Clin Invest* **125**, 4572-4586 (2015).

73. Murtomaki, A. *et al.* Notch1 functions as a negative regulator of lymphatic endothelial cell differentiation in the venous endothelium. *Development* **140**, 2365-2376 (2013).

74. Geng, X. *et al.* S1PR1 regulates the quiescence of lymphatic vessels by inhibiting laminar shear stress-dependent VEGF-C signaling. *JCI Insight* **5** (2020).

75. Aspelund, A. *et al.* The Schlemm's canal is a VEGF-C/VEGFR-3-responsive lymphatic-like vessel. *J Clin Invest* **124**, 3975-3986 (2014).

76. Lin, M.I., Yu, J., Murata, T. & Sessa, W.C. Caveolin-1-deficient mice have increased tumor microvascular permeability, angiogenesis, and growth. *Cancer Res* **67**, 2849-2856 (2007).

77. Hamada, K. *et al.* VEGF-C signaling pathways through VEGFR-2 and VEGFR-3 in vasculoangiogenesis and hematopoiesis. *Blood* **96**, 3793-3800 (2000).

78. Liang, D. *et al.* The role of vascular endothelial growth factor (VEGF) in vasculogenesis, angiogenesis, and hematopoiesis in zebrafish development. *Mech Dev* **108**, 29-43 (2001).

79. Martinez-Corral, I. *et al.* Nonvenous origin of dermal lymphatic vasculature. *Circ Res* **116**, 1649-1654 (2015).

80. Mortimer, P.S. & Rockson, S.G. New developments in clinical aspects of lymphatic disease. *J Clin Invest* **124**, 915-921 (2014).

81. Brouillard, P., Boon, L. & Vikkula, M. Genetics of lymphatic anomalies. *J Clin Invest* **124**, 898-904 (2014).

82. Jao, L.-E., Wente, S.R. & Chen, W. Efficient multiplex biallelic zebrafish genome editing using a CRISPR nuclease system. *Proc Natl Acad Sci U S A* **110**, 13904-13909 (2013).

83. Tsang, K.M. *et al.* Embryonic stem cell differentiation to functional arterial endothelial cells through sequential activation of ETV2 and NOTCH1 signaling by HIF1α. *Stem cell reports* **9**, 796-806 (2017).

Figure legends

Figure 1. Effect of Aibp2 knockout on lymphatic vessel development and LEC fate specification. A, Lymphatic developmental defects in *apoa1bp2*$^{-/-}$ zebrafish. Maxi-projection confocal images of TD formation in the *fli1a:egfp* and *apoa1bp*$^{-/-}$*; fli1a:egfp* null zebrafish at 5 dpf. Arrows show the TD, and stars denote absent TD. **B**, Quantitative data of TD formation in A. n=15. **C**, Loss of Aibp2 disrupts PL formation in *fli1a:egfp* zebrafish. Confocal images of PL in the horizontal myoseptum at 48 hpf. Arrows indicates PLs, and stars show absent PLs. **D**, Quantitative data of the PL string in C. n=20. **E**, Impaired LEC specification in *apoa1bp*$^{-/-}$*; fli1a:egfp* zebrafish. Control and *apoa1bp2* knockout zebrafish were fixed with 4% PFA at 36 hpf, whole mount immunostaining was performed using Prox1 and EGFP antibodies, and images were captured using confocal microscopy. **F**, Enumeration of LEC progenitors in panel E. Arrows show specified LEC progenitors. **G**, Scheme illustration of mESC to LEC differentiation. **H**&**K,** AIBP augments LEC differentiation from mESCs. The embryoid bodies (EBs) of mESCs were prepared and cultured in the EC differentiation medium containing 2 ng/ml BMP4 and 10 ng/ml bFGF for 3 days. Recombinant VEGFA (50 ng/ml) and VEGFC (50 ng/ml) in combination or AIBP (100 ng/ml) alone were supplemented at day 3 and kept in culture for additional 4 days. The resulting cells were harvested for qPCR analysis of endothelial cell (EC) marker *Pecam1* expression (**H**) and LEC-associated *Lyve1* expression (**I**) at the indicated time points. Western blot analyses of PECAM1, LYVE1 and PROX1 expression (**J**) and the quantitative data (**K**). C: control; V: VEGFA + VEGFC; A: AIBP. *, $p<0.05$; **, $p<0.001$; ****, $p<0.0001$. Scale: 25 μm.

Figure. 2. Effect of cholesterol reduction on lymphatic vessel development. (**A**) Free cholesterol (FC) content in control and Aibp2 null zebrafish. The 5 dpf zebrafish trunk of control or Aibp2 null zebrafish were dissected, total lipids extracted, and free cholesterol levels measured. The FC content were normalized to the protein levels. Fifty embryos were pooled for each measurement. Mean±SE; *, $p<0.05$. (**B**) Inhibition of cholesterol synthesis rescues TD formation

in Aibp2 null animals. TD formation in control zebrafish, Aibp2 null zebrafish treated with 1 μM atorvastatin or control vehicle ethanol at 5 dpf. (**C**) Quantitative data of TD formation in B. n=20. (**D**) ApoA1-mediated cholesterol efflux restores TD formation. Confocal images of TD formation in control zebrafish, Aibp2 null zebrafish, or Aibp2 knockout zebrafish with 100 ng human *APOA1* mRNA overexpression. (**E**) Quantitative data of TD formation in D. Arrows show TD, and stars denote absent TD. n=18. Scale: 25 μm. *, $p<0.05$ using student *t*-test.

Figure. 3. Effect of cholesterol efflux on VEGFR3 signaling. A & **B**. Cholesterol removal potentiates VEGFR3 signaling. **A**, hLECs were serum-starved, and treated with 10 mM MβCD for 30 min, and cells were further stimulated with 100 ng/ml VEGFC. The resulting cells were lysed and blotted with Cav-1 or GAPDH antibodies. **B,** hLECs were treated as in (**A**). and cell lysates were immunoprecipitated using VEGFR3 antibody. Immunoblotting was performed using anti-phosphotyrosine (4G10) and VEGFR3 antibodies. **C,** AIBP-mediated cholesterol efflux disrupts caveolae and reduces CAV-1 levels in the caveolar fractions. hLECs were treated with recombinant 200 ng/ml AIBP, 100 μg/ml HDL_3, or both in serum-free EBM2 for 6 hours, and the cells were subjected to sucrose-mediated ultracentrifugation. The resulting fractions were collected for Western blot analysis as indicated. **D,** AIBP-mediated cholesterol efflux increases VEGFR3 signaling. hLECs were serum-starved and treated as in (**C**), and further stimulated with 100 ng/ml VEGFC. The resulting cells were lyzed and immunoblotted as indicated. **E** & **F**, Quantitative data of AKT activation (**E**) and ERK activation (**F**). Mean±SD, n=3 independent repeats. *, $p<0.05$; **, $p<0.01$; ns: not significant using student *t*-test.

Figure. 4. Effect of CAV-1 on VEGFR3 signaling. A, Conserved CAV-1 binding site on VEGFR3 in human (Hu), mouse (Ms), and zebrafish (Zf). **B,** $VEGFR3^{AAA}$ loses its binding to CAV-1. hLECs were transfected with control EGFP (Ctrl), VEGFR3-EGFP (R3), or $VEGFR3^{AAA}$-EGFP ($R3^{AAA}$)

using lentivirus-mediated gene transfer. After 72 hours, the resulting cells were lyzed and immunoprecipitated with EGFP antibody coupled to the magnetic Dynabeads and immunoblotted using VEGFR3 and CAV-1 antibodies. Immunoblotting of overexpressed VEGFR3-EGFP and VEGFR3^{AAA}-EGFP (R3/R3^{AAA}-EGFP) were detected using VEGFR3 antibody. The input lysates were shown on the right. **C,** VEGFR3^{AAA} increases VEGFR3 signaling. hLECs were transduced as in (**B**), and the resulting cells were serum starved and treated with 100 ng/ml VEGFC for 20 min, cells were then lysed and immunoblotted as indicated. Quantitative data of VEGFR3 activation (**D**), AKT activation (**E**), and ERK activation (**F**) were shown. n=3 independent repeats. *, $p<0.05$; **, $p<0.01$; and ***, $p<0.001$ using student *t*-test.

Figure. 5. Effect of CAV-1 on Aibp2-regulated LEC specification. A, Cav-1 deficiency rescues LEC specification in Aibp2 knockdown animals. Max projection confocal images of control, Aibp2-deficient, Cav-1 null, or Cav-1/Aibp2 double deficient zebrafish. The animals were PFA fixed at 36 hpf and immunostained using Prox1 and EGFP antibodies. Arrows indicate LEC progenitors. **B**, Quantitative data of LEC progenitors in (**A**). **C** Cav-1 deficiency corrects lymphatic defects in Aibp2 knockdown animals. Confocal imaging of TD formation in the indicated genetically modified *fli1a:egfp* zebrafish at 5 dpf. Arrows show TD, and stars denote absent TD. **D** Quantitative data of TD formation in (**C**). **, $p<0.01$; ****, $p<0.0001$; ns: not significant when compared with control using one-way ANOVA analysis, n=20. **E**, Confocal imaging of TD at 3.5 dpf zebrafish in the indicated zebrafish. **F**, Quantification of TD length in 7 somite. *, $p<0.05$; **, $p<0.01$; ****, $p<0.0001$; ns: not significant. Scale: 25 μm.

Figure. 6. AIBP effect on corneal lymphangiogenesis and LEC specification. A, Illustration of murine cornea lymphangiogenesis assay. **B,** Representative images of murine corneal lymphangiogenesis by implantation of pellets containing the indicated recombinant proteins and immunostained using LYVE1 & CD31 antibodies. Enlarged images of the boxed regions (scale

bar, 1000 μm) are shown in the lower panels (scale bar, 500 μm). **C,** Quantification of LYVE1+ lymphatic vessel area per cornea. VC: VEGFC; AA: AIBP+APOA1; CSD: CAV-1 scaffolding domain peptide. *, $p<0.05$; **, $p<0.01$ by one-way ANOVA analysis.

Figure. 7. Effects of AIBP and CSD on the VEGFC-facilitated recovery from lymphedema in mice. A, One year old mice were subjected to tail surgery to create lymphedema. Immediately following the surgery, recombinant human VEGFC (0.2 μg/mouse), VEGFC in combination with AIBP (1 μg/mouse) or CSD (1 μg/mouse), or saline control were delivered via peritoneal injection, twice a week for 4 weeks. The tails were imaged every 7 days after the injury, and the recovery from swelling analyzed. **B,** The quantification of tail volume in panel **A**. The curve illustrates a fitness of beta growth then decay. (**C-F**) AIBP expression in cutaneous lymphedema. **C,** Immunohistochemistry analysis of AIBP expression. Paired normal and lymphedema cutaneous biopsies (n=7 patients) were fixed with formalin and the 5 μm paraffin sections were prepared. The sections were deparaffinized and immunostained using our non-commercial AIBP antibody. The AIBP signal in the epidermis (**D**), dermis (**E**), and sweat glands (**F**) were quantified using ImageJ. The enlarged areas of green and yellow boxes are shown on the right. The images were taken separately and stitched together using the EVOS microscope. *, $p<0.05$; ns: not significant using one-way ANOVA analysis in panel **B**; and **, $p<0.01$ using student *t*-test in panel **D-F**. NL: normal leg (paired control); LY: lymphedema.

Figures

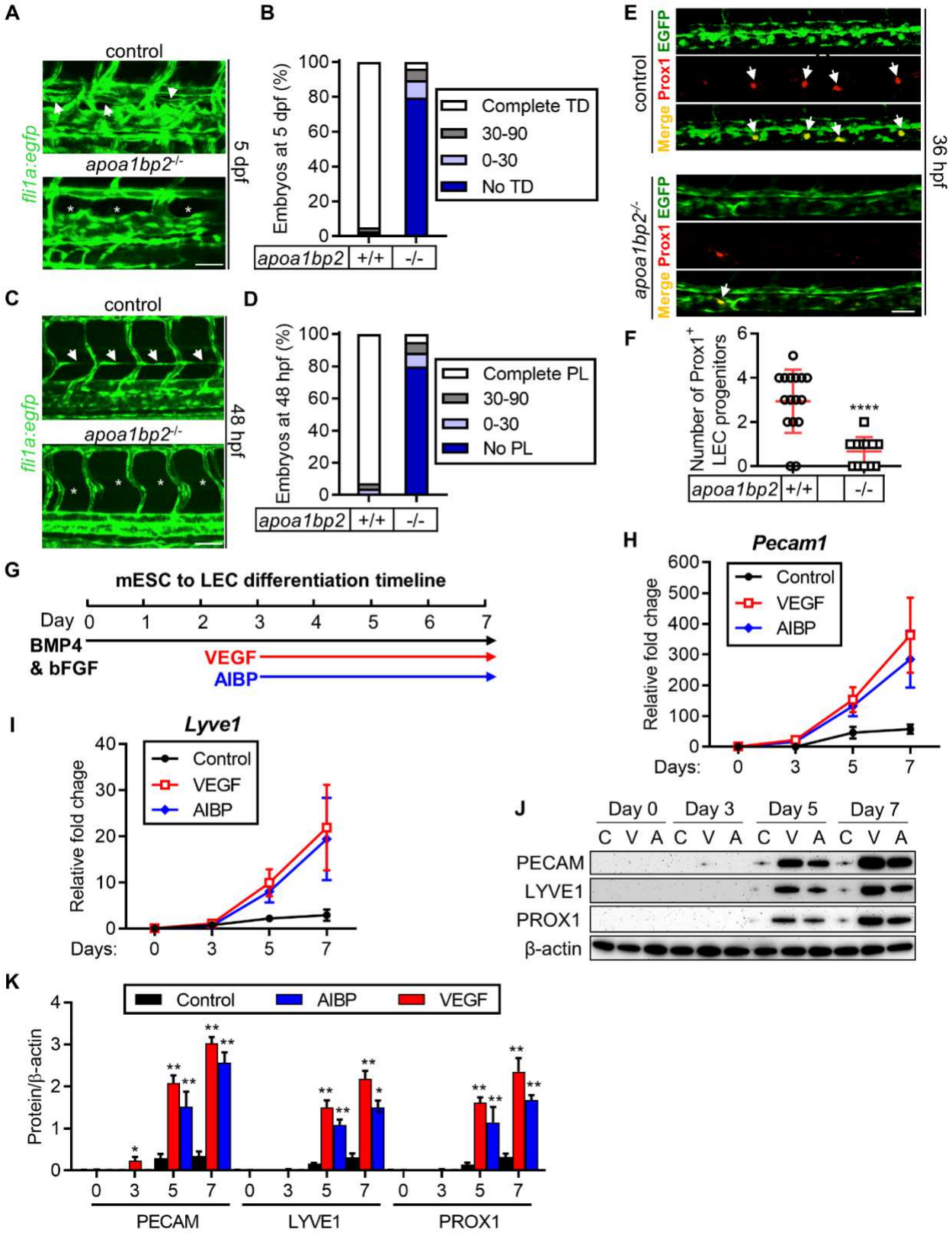
A
control
fli1a:egfp
apoa1bp2-/-
5 dpf
B
Embryos at 5 dpf (%)
Complete TD
30-90
0-30
No TD
apoa1bp2 +/+ -/-
C
control
fli1a:egfp
apoa1bp2-/-
48 hpf
D
Embryos at 48 hpf (%)
Complete PL
30-90
0-30
No PL
apoa1bp2 +/+ -/-
E
control
Merge Prox1 EGFP
apoa1bp2-/-
36 hpf
F
Number of Prox1+ LEC progenitors
****
apoa1bp2 +/+ -/-
G
mESC to LEC differentiation timeline
Day 0 1 2 3 4 5 6 7
BMP4 & bFGF
VEGF
AIBP
H
Pecam1
Relative fold chage
Control
VEGF
AIBP
Days: 0 3 5 7
I
Lyve1
Relative fold chage
Control
VEGF
AIBP
Days: 0 3 5 7
J
Day 0 Day 3 Day 5 Day 7
C V A C V A C V A C V A
PECAM
LYVE1
PROX1
β-actin
K
Control AIBP VEGF
Protein/β-actin
PECAM LYVE1 PROX1

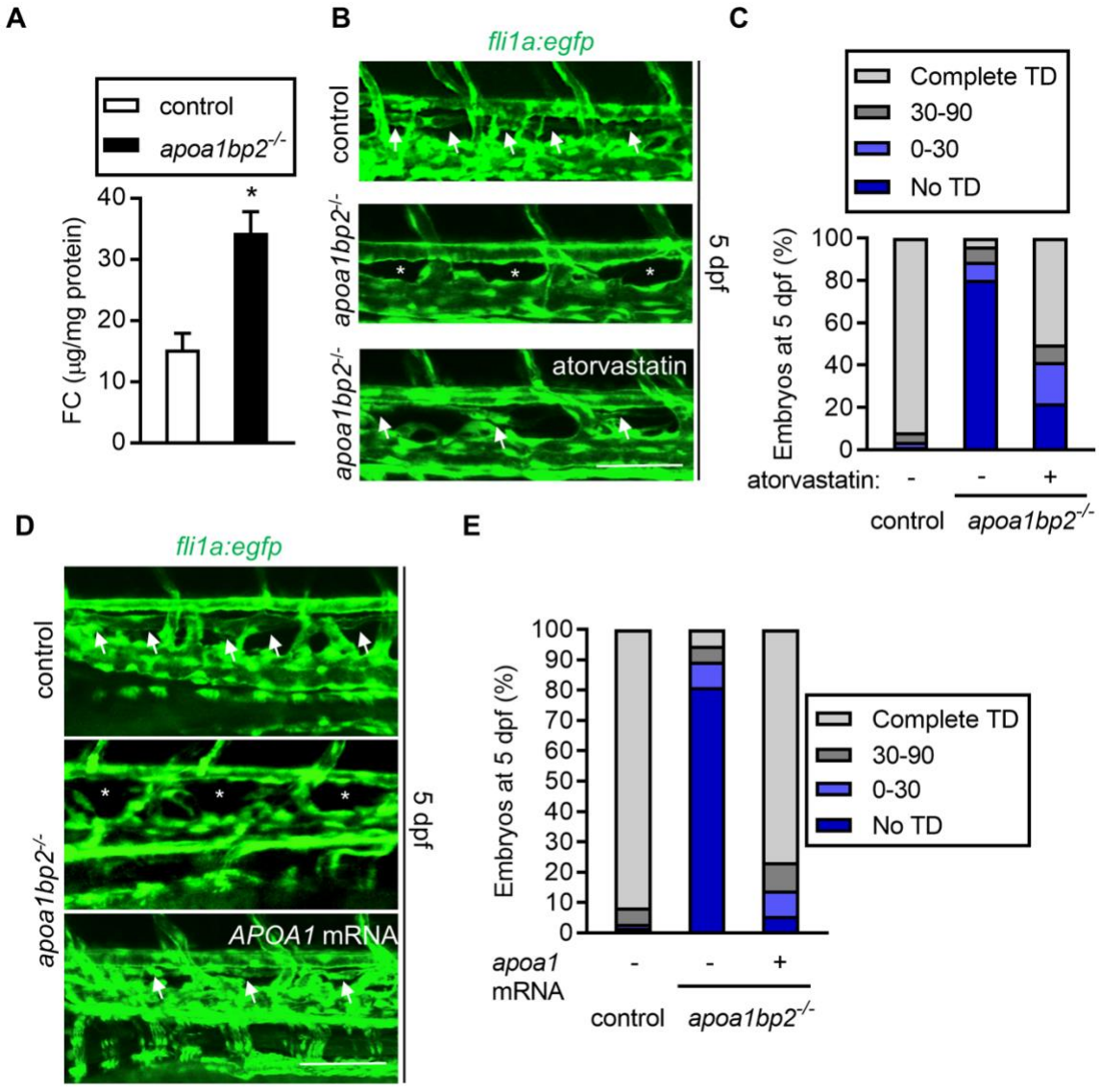
A
control
apoa1bp2-/-
FC (µg/mg protein)
40
30
20
10
0
*
B
fli1a:egfp
control
apoa1bp2-/-
apoa1bp2-/-
atorvastatin
5 dpf
C
Complete TD
30-90
0-30
No TD
Embryos at 5 dpf (%)
100
80
60
40
20
0
atorvastatin: - - +
control
apoa1bp2-/-
D
fli1a:egfp
control
apoa1bp2-/-
APOA1 mRNA
5 dpf
E
Embryos at 5 dpf (%)
100
90
80
70
60
50
40
30
20
10
0
Complete TD
30-90
0-30
No TD
apoa1 mRNA - - +
control
apoa1bp2-/-

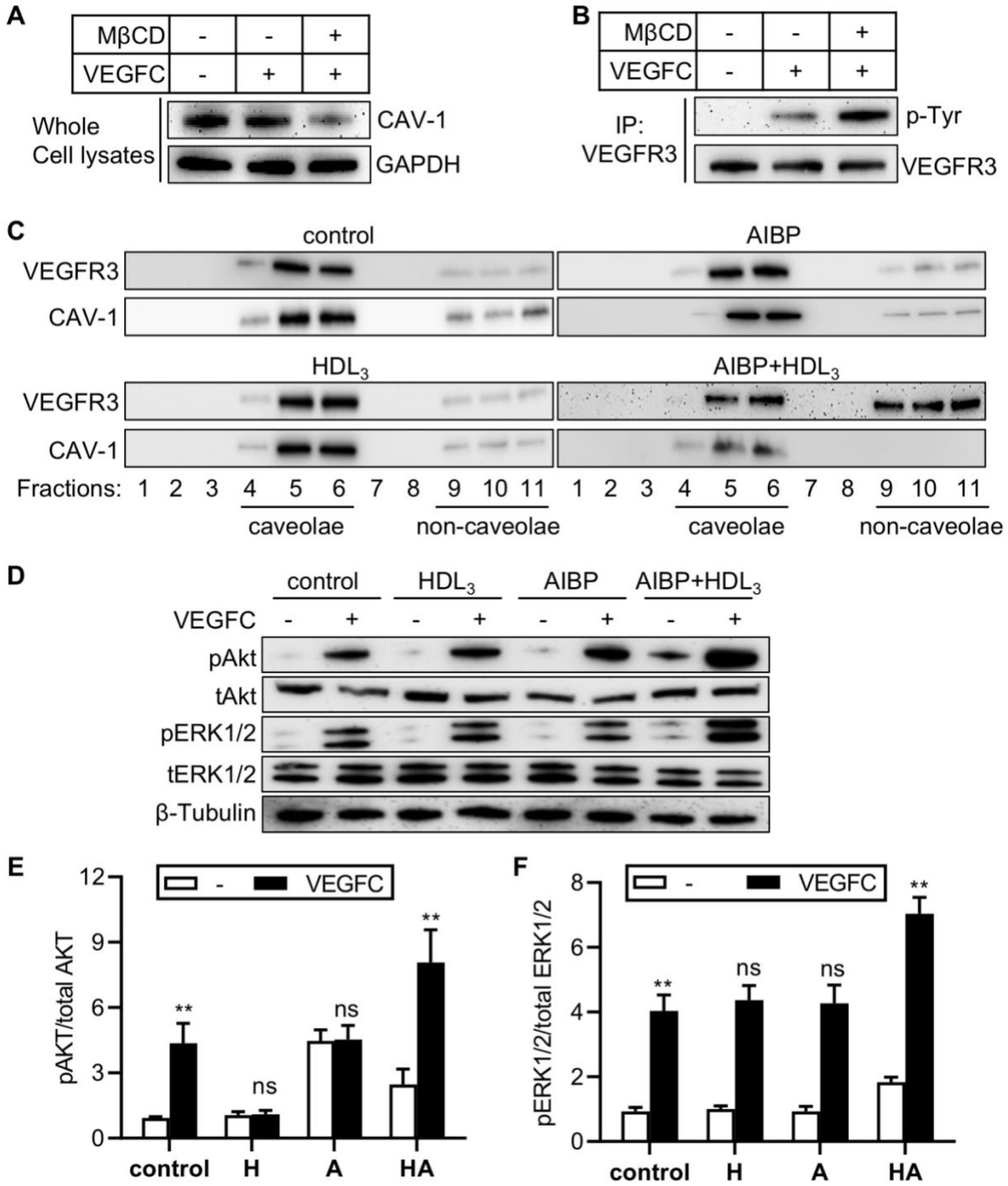
A
MβCD - - +
VEGFC - + +
Whole Cell lysates
CAV-1
GAPDH
B
MβCD - - +
VEGFC - + +
IP: VEGFR3
p-Tyr
VEGFR3
C
control
AIBP
VEGFR3
CAV-1
HDL3
AIBP+HDL3
VEGFR3
CAV-1
Fractions: 1 2 3 4 5 6 7 8 9 10 11 1 2 3 4 5 6 7 8 9 10 11
caveolae
non-caveolae
caveolae
non-caveolae
D
control
HDL3
AIBP
AIBP+HDL3
VEGFC - + - + - + - +
pAkt
tAkt
pERK1/2
tERK1/2
β-Tubulin
E
- VEGFC
pAKT/total AKT
12
9
6
3
0
**
ns
ns
**
control
H
A
HA
F
- VEGFC
pERK1/2/total ERK1/2
8
6
4
2
0
**
ns
ns
**
control
H
A
HA

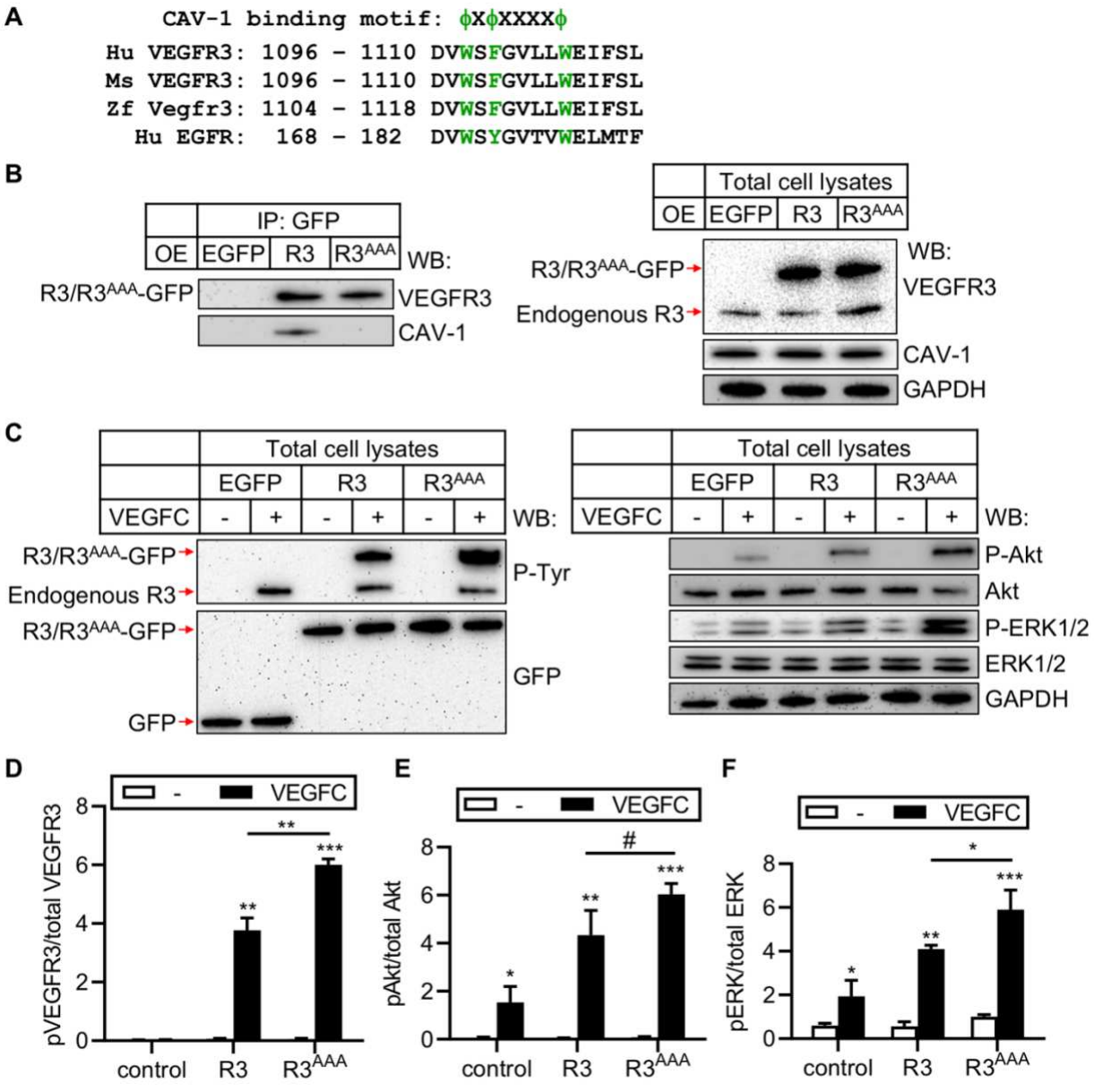
A
CAV-1 binding motif: ϕXϕXXXXϕ
Hu VEGFR3: 1096 – 1110 DVWSFGVLLWEIFSL
Ms VEGFR3: 1096 – 1110 DVWSFGVLLWEIFSL
Zf Vegfr3: 1104 – 1118 DVWSFGVLLWEIFSL
Hu EGFR: 168 – 182 DVWSYGVTVWELMTF
B
IP: GFP
OE
EGFP
R3
R3AAA
WB:
R3/R3AAA-GFP
VEGFR3
CAV-1
Total cell lysates
OE
EGFP
R3
R3AAA
R3/R3AAA-GFP
Endogenous R3
WB:
VEGFR3
CAV-1
GAPDH
C
Total cell lysates
EGFP
R3
R3AAA
VEGFC
-
+
WB:
R3/R3AAA-GFP
Endogenous R3
P-Tyr
GFP
P-Akt
Akt
P-ERK1/2
ERK1/2
GAPDH
D
VEGFC
pVEGFR3/total VEGFR3
control
R3
R3AAA
E
pAkt/total Akt
F
pERK/total ERK

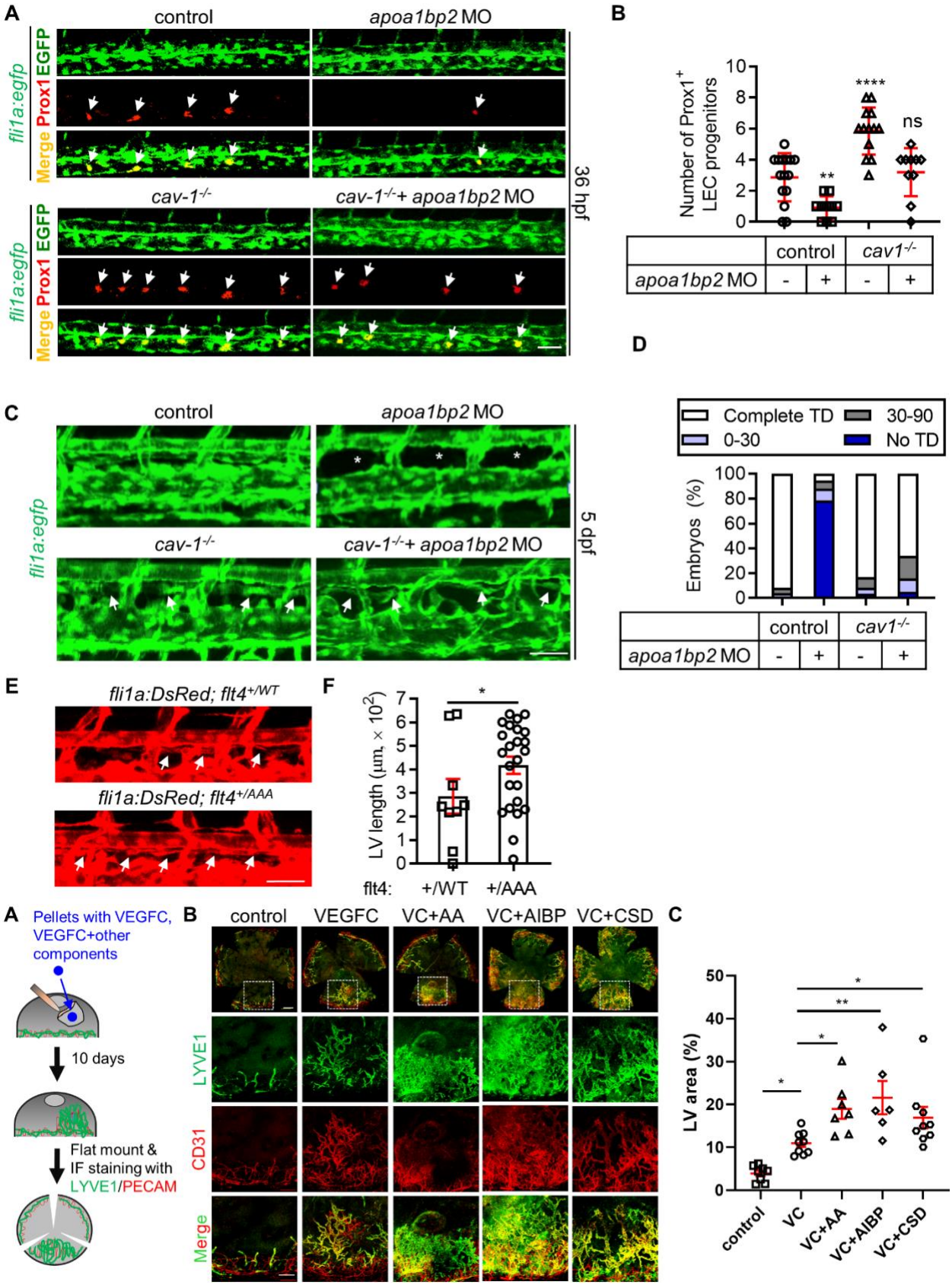
A
control
apoa1bp2 MO
fli1a:egfp
EGFP Prox1 Merge
cav-1-/-
cav-1-/-+ apoa1bp2 MO
36 hpf
B
Number of Prox1+ LEC progenitors
control
cav1-/-
apoa1bp2 MO
C
5 dpf
D
Complete TD
30-90
0-30
No TD
Embryos (%)
E
fli1a:DsRed; flt4+/WT
fli1a:DsRed; flt4+/AAA
F
LV length (μm, × 10-2)
flt4: +/WT +/AAA
A
Pellets with VEGFC, VEGFC+other components
10 days
Flat mount & IF staining with LYVE1/PECAM
B
control
VEGFC
VC+AA
VC+AIBP
VC+CSD
LYVE1
CD31
Merge
C
LV area (%)
control
VC
VC+AA
VC+AIBP
VC+CSD

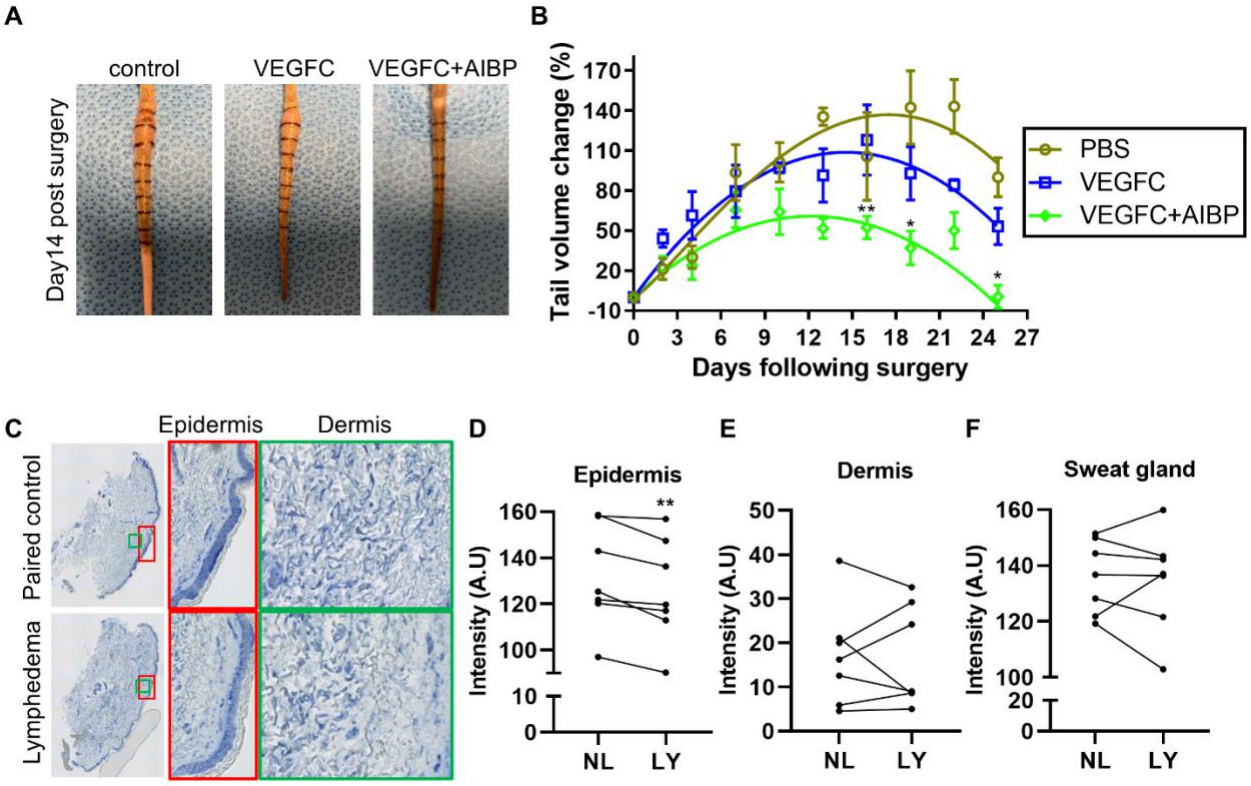
A
control
VEGFC
VEGFC+AIBP
Day14 post surgery
B
Tail volume change (%)
Days following surgery
PBS
VEGFC
VEGFC+AIBP
C
Epidermis
Dermis
Paired control
Lymphedema
D
Epidermis
E
Dermis
F
Sweat gland
Intensity (A.U)
NL
LY

Supplementary Information

AIBP-CAV1-VEGFR3 axis dictates lymphatic cell fate and controls lymphangiogenesis

Xiaojie Yang[1,9], Jun-dae Kim[1,9*], Siu-Lung Chan[2], Qilin Gu[1], Jonathan Astin[3], Philip S Crosier[3], Pengchun Yu[4], Stanley G Rockson[5], Hong Chen[2,*], and Longhou Fang[1,6,7,8,*]

[1]Center for Cardiovascular Regeneration, Department of Cardiovascular Sciences, Houston Methodist Research Institute. Houston Methodist, 6550 Fannin Street, Texas 77030, USA.

[2]Vascular Biology Program, Boston Children's Hospital, Harvard Medical School, Boston, MA 02115, USA

[3]Department of Molecular Medicine & Pathology, School of Medical Sciences, University of Auckland, Auckland 92019, New Zealand.

[4]Cardiovascular Biology Research Program, Oklahoma Medical Research Foundation 825 N.E. 13th Street Oklahoma City, OK 73104.

[5]Center for Lymphatic and Venous Disorders, Stanford University School of Medicine, 300 Pasteur Drive, Stanford, CA 94305.

[6]Department of Ophthalmology-Blanton Eye Institute,

[7]Houston Methodist Institute for Academic Medicine, Houston Methodist Research Institute. Houston Methodist, 6550 Fannin Street, Texas 77030, USA.

[8]Department of Cardiothoracic Surgeries, Weill Cornell Medical College, Cornell University, New York 10065, USA.

[9]Contributed equally

*correspondence: Jkim3@houstonmethodist.org, hong.chen@childrens.harvard.edu, or lhfang@houstonmethodist.org.

Supplemental Figures

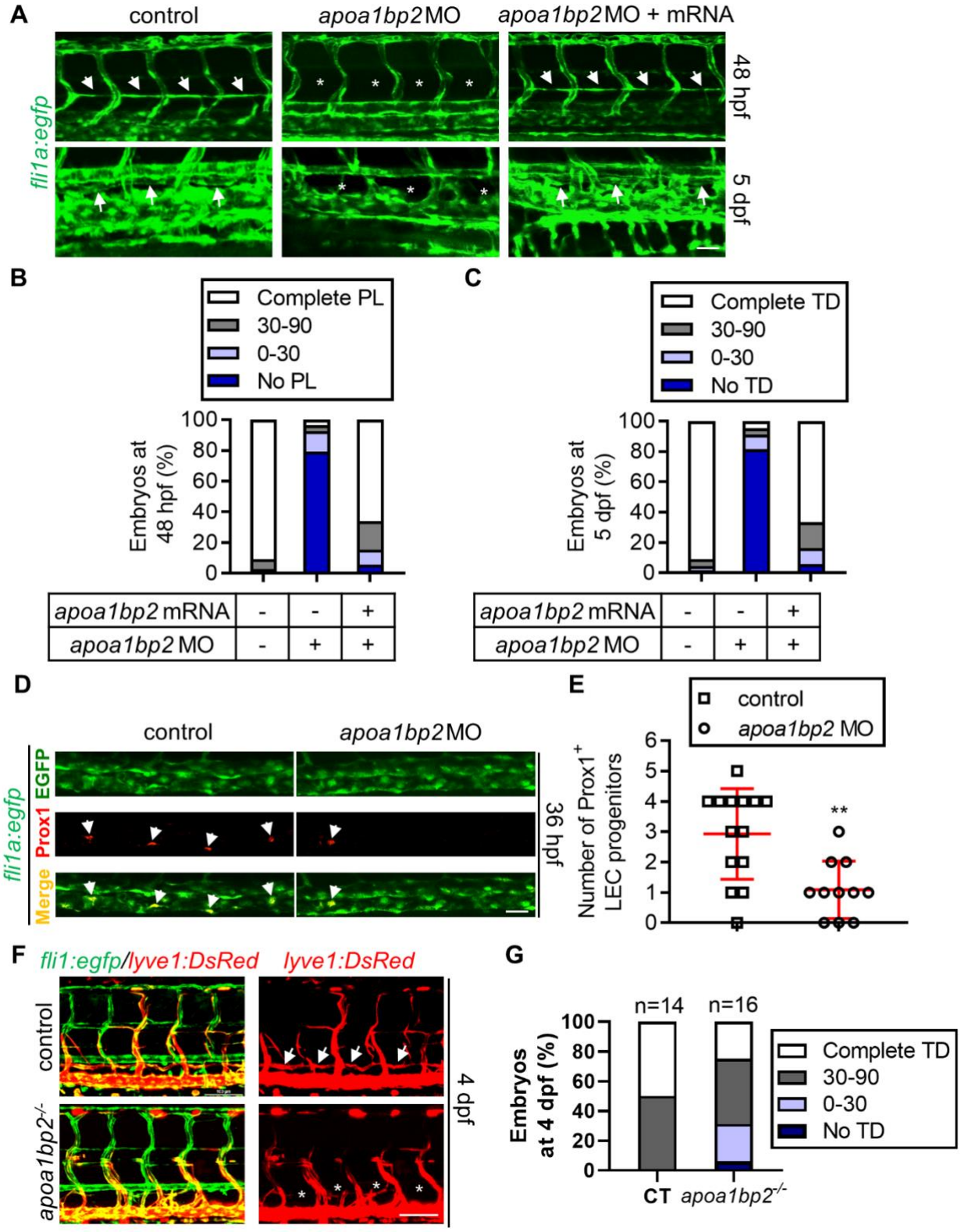

Figure. S1. **AIBP regulates lymphatic vessel development in zebrafish. A**, Lymphatic developmental defects in Aibp2 knockdown zebrafish. Confocal images of PL at 48 hpf and TD formation at 5 dpf in the control and Aibp2 null zebrafish. Arrows show PL or TD, and stars denote absent PL or TD. Quantitative data of PL (**B**) and TD formation (**C**) in A. n=25 in panel A and n=30 in panel C. Arrows indicate LECs. **D**, Aibp2 ablation disrupts LEC specification. Confocal images of LEC progenitors in the CV of control or Aibp2 knockdown zebrafish at 36 hpf. **E**, Quantitative data of LEC progenitors in panel A. Control or *apoa1bp2* morphants were fixed at 36 hpf, immunostained using Prox1 and EGFP antibodies, and images were captured using confocal microscopy. Arrows indicate LEC progenitors. **F**&**G**, TD development in *apoa1bp2*$^{-/-}$ and control (CT) *lyve1:DsRed* zebrafish (**F**) and the quantification (**G**). Scale: 25 μm. **, $p<0.01$. Scale bar: 100 μm.

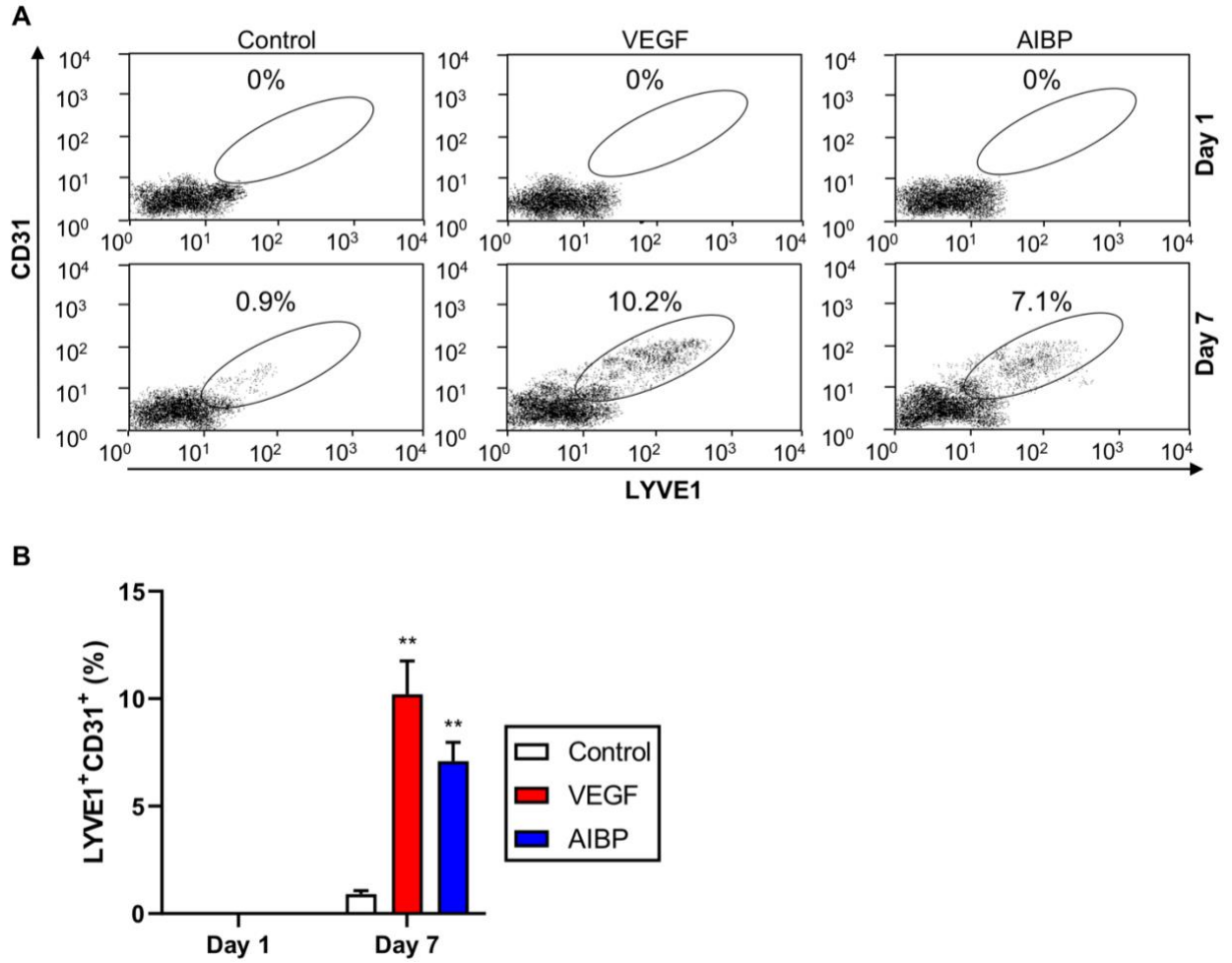

Figure. S2. FACS analysis of murine ESC-derived CD31⁺LYVE1⁺ LECs. (**A**) AIBP induces LEC lineage commitment from mESCs. The murine ESCs were subjected to mesoderm and then endothelial differentiation as described in **Fig. 2C**. At day 1 and day 7, the resulting cells were dissociated, immunostained with CD31 and LYVE1 antibodies, fixed with 4% PFA, and used for FACS analysis. The percentage of $CD31^+$ and $LYVE1^+$ cells were shown. (**B**) Quantitative data of FACS-sorted $CD31^+$ and $LYVE1^+$ cells in panel (A). **p<0.01.

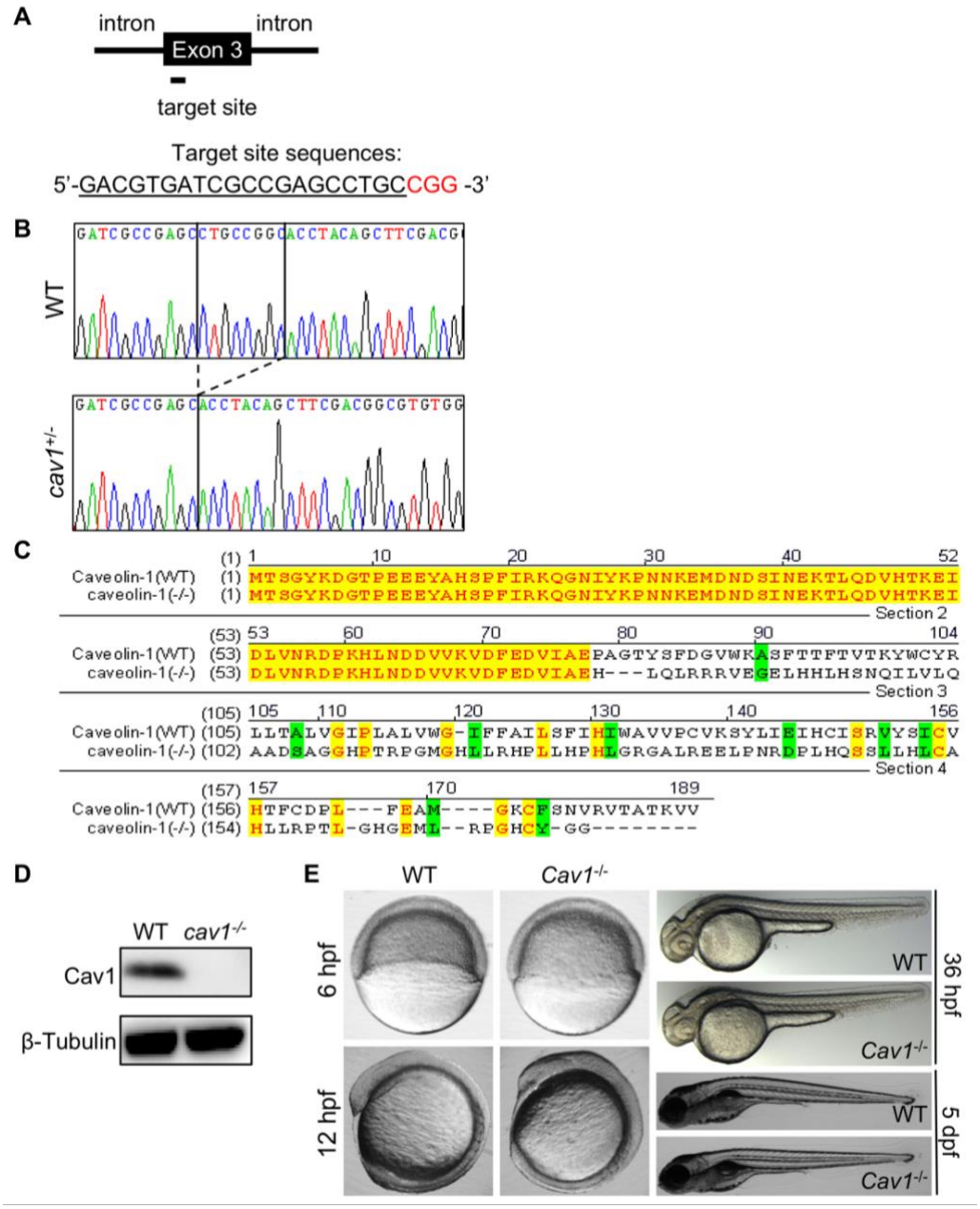

Figure. S3. Generation of Cav-1 knockout zebrafish. (**A**) Diagram showing position of the target site and its sequence (underline) in zebrafish *apoa1bp2* locus. PAM sequence (GGG) is shown in red. (**B**) Sanger sequencing result of heterozygous mutants revealed an 8-bp genomic DNA fragment insertion from the target site. The PCR amplicons that span the mutated *apoa1bp2* region were ligated into a T-vector and subsequently transformed into competent cells. Single positive colonies were selected for sequencing. (**C**) The 8-bp insertion resulted in a frame shift

that generates a mutated protein. (**D**) Western analysis of pooled 26 hpf zebrafish (n=15) show the absence of Cav-1 expression. (**E**) No gross phenotypic defect observed in Cav-1 knockout zebrafish. Zebrafish embryos at the indicated developmental stages were collected and images of live zebrafish embryos captured. hpf: hour(s) post fertilization. dpf: days post-fertilization. WT: wild type.

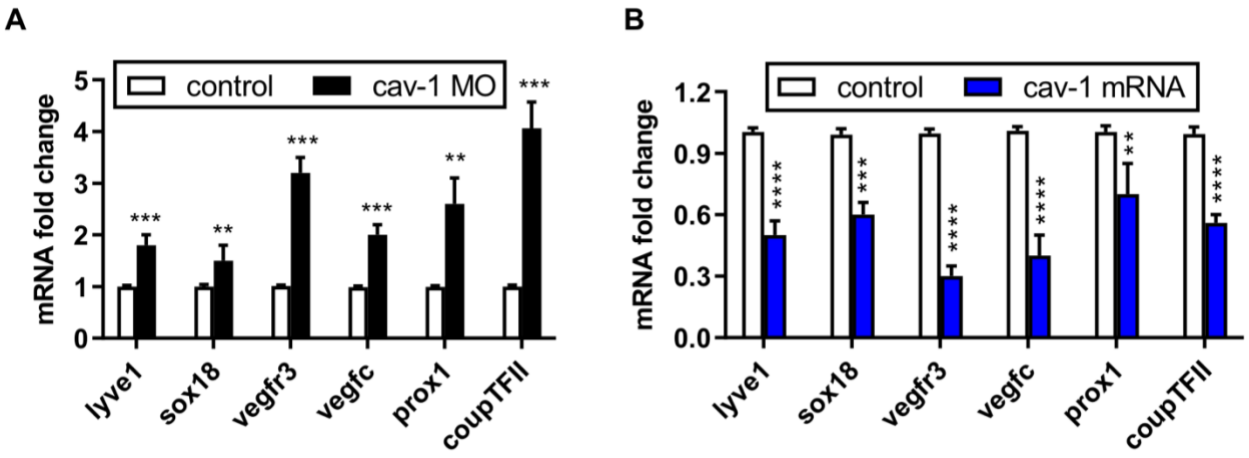

Figure. S4. Quantitative PCR analysis of genes regulating lymphatic development in zebrafish. (**A**) Loss of Cav-1 increases LEC gene expression. qPCR analysis of the indicated genes regulating lymphangiogenesis in control and Cav-1 null zebrafish at 96 hpf. (**B**) Cav-1 overexpression reduces LEC gene expression. The zebrafish embryo at one cell stage was injected with Cav-1 mRNA, and the resulting animals or control animals were harvested at 96 hpf, and total RNA extracted for reverse transcription. The indicated genes regulating lymphangiogenesis were analyzed using qPCR in control and Cav-1 overexpressing zebrafish. n=30 per sample. **, p<0.01; ***, p<0.001; ****, p<0.0001.

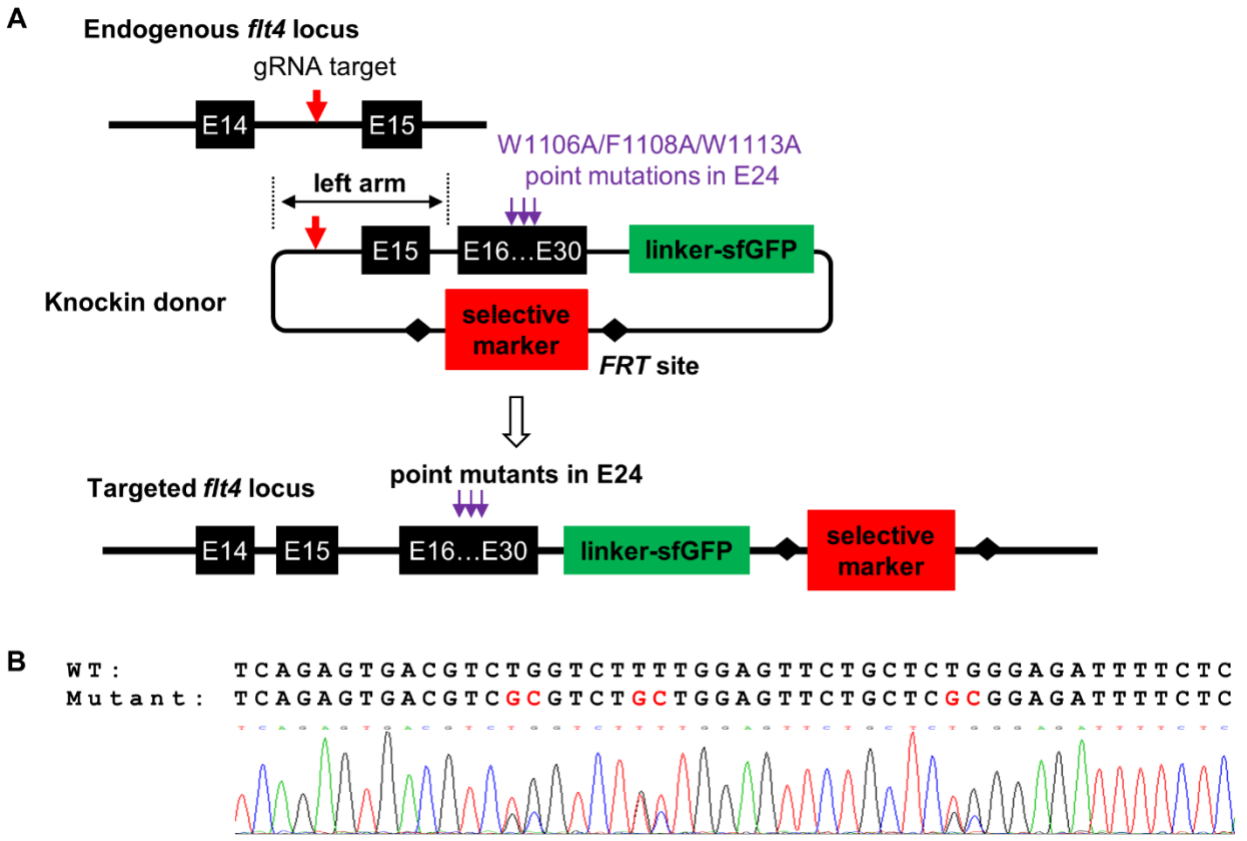

Figure. S5. Generation of the knockin zebrafish with Flt4 mutant deficient in binding Cav-1. A. gRNA-mediated cutting at the intron between Exon (E)14 and E15 facilitates the integration of the knockin mutant donor, which contains 3 repeats of GGGGS linker sfGFP. The resulting Vegfr^{AAA} will have the sfGFP tag. In this construct, we engineered DsRed expression in the heart for the purpose of selection. **B**. DNA-sequencing verified the mutation in the F1 embryos. We isolated mRNA and reversely transcribed to cDNA, the resulting Cav-1 binding domain was amplified and sequenced. sfGFP: superfolder GFP.

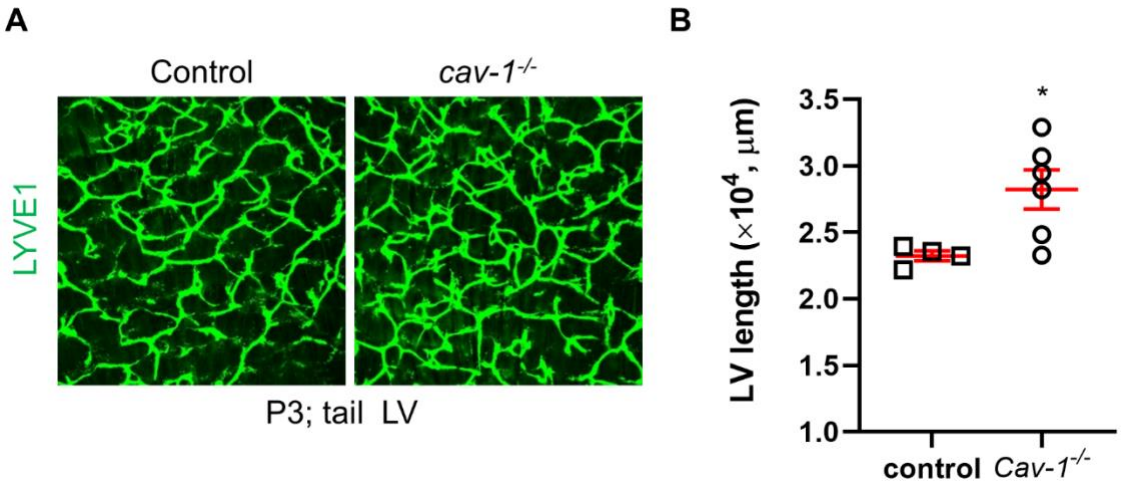

Figure. S6. CAV-1 knockout increases tail lymphangiogenesis in neonatal mice. (**A**) The CAV-1 knockout mice were purchased from JAX (stock No. 007083). The tail epidermis of CAV-1 knockout mice and control littermates were dissected from the similar anatomical locations and immunostained using LYVE-1 antibodies. (**B**) Quantification of lymphatic vessel length in panel (A) were performed using ImageJ. *, $p<0.05$.

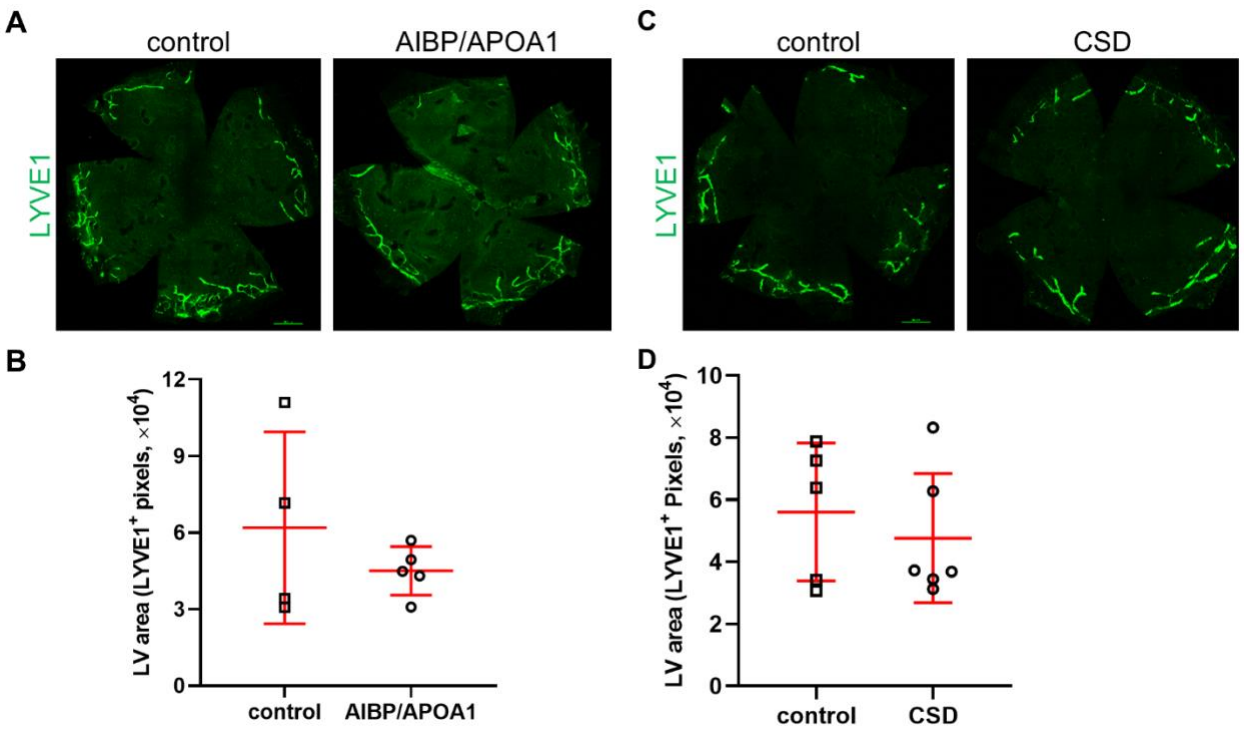

Figure. S7. AIBP/APOA1 or CSD per se has no effect on adult lymphangiogenesis. (**A** and **C**)**,** PEG pellets containing recombinant AIBP and APOA1 were prepared and implanted into the corneas of C57BL/6 mice, control was implanted with control pellets. (**C** and **D**)**,** Quantification of lymphatic vessel area in panel (**A** and **C**).